Inward tubulation of the plasma membrane expedites membrane exchange and receptor presentation

Long-fang Yao [1], Li Zhou [1], Ruiling Zhang [1], Liang Cai [1,2]

[1] School of Life Sciences, Fudan University, Shanghai, China 200438
[2] The Center for Faculty Development of Fudan University, Shanghai, China

Correspondence to: L Cai, cail@fudan.edu.cn

Abstract

The plasma membrane is a crucial barrier between the cell and its external environment, and it also enables efficient passage of materials and information. Membrane vesicle trafficking allows precise delivery of materials but is rather inefficient. The mechanism for efficient membrane exchange remains elusive. Here we describe inward tubulation of the plasma membrane (PM tubes) that extends deep into the cytoplasm. These widespread PM tubes elongate along microtubules and are stabilized by actin filaments and cholesterol. PM tubes are preferred sites for connection between the endoplasmic reticulum and the plasma membrane. PM tubes facilitate receptor presentation at the surface of cells, possibly also shortening the distance for transported cargo to reach the external environment.

In Brief

A new type of tubular membrane structures was discovered in cells, revealing a shortcut that cells employ to expedite material exchange with their external environment.

Highlights

- Inward tubulation of the plasma membrane (PM tubes), transiently interacts with the Golgi apparatus
- Microtubule side-binding proteins pull PM tubes, while actin filaments and cholesterol stabilize PM tubes
- PM tubes are preferred sites where ER-PM contacts form in response to increased cytoplasmic calcium concentration
- PM tubes are preferred sites for the surface presentation of GLUT1 upon glucose deprivation

Introduction

All reactions take place in their specific environment, usually within limited space and time. For cells, biological membrane-bound organelles are where all cellular reactions take place. '*Omnis membrane e membrane*', what Günter Blobel addressed in 1999 highlights the principle of membrane biogenesis (Blobel, 2000), as well as the challenge the eukaryotic cells must overcome, that is, to exchange material, including cargos and membranes, precisely and efficiently between organelles.

The benefit of compartmentalized cellular structures allows the cells to have specialized space to execute specialized reactions efficiently, i.e., the nucleus for storage and transmission of genetic information, lysosomes for recycling material, mitochondria and chloroplasts for energy metabolism, endoplasmic reticulum (ER) and Golgi apparatus for protein synthesis and maturation. Most if not all biological reactions happen in membrane-bound organelles, and membranes not only function as barriers between the cell and its external environment but also provide a physical platform for various reactions (Lippincott-Schwartz, 2011; Steinman et al., 1983).

Besides direct interactions, membrane vesicle trafficking is thought to be the only approach to exchange materials between membrane-bound compartments. Certain materials, usually called cargos, are packaged into vesicles, bound by the source membrane, and depart from the source compartment. These vesicles are transported by motor proteins along tracks formed by cytoskeletal filaments. When the cargo-containing vesicles reach the target compartment, the vesicle membrane fuses with the target membrane, and the cargos are released. Simultaneously, the source membrane is being delivered to the target compartment. In eukaryotic cells, material exchange between the compartments is achieved by membrane vesicle trafficking, including transports between organelles, and between the internal and the external environment of the cell. Years of studies in many laboratories around the world have tempted to illustrate detailed mechanisms of almost every aspect of membrane vesicle trafficking (Bonifacino and Glick, 2004; Hutagalung and Novick, 2011; Lippincott-Schwartz et al., 2000). However, the question how to achieve efficient transportation of material, especially membrane, between compartments is still elusive.

Recently, various membrane contact sites have been reported (Chinnapen et al., 2012; Friedman et al., 2011; Giordano et al., 2013; Manford et al., 2012; Rowland

et al., 2014; Stefan et al., 2011; Tavassoli et al., 2013). Most of these structures are formed between ER and other membrane-bound organelles, e.g., mitochondria, peroxisomes, and the plasma membrane. These reported structures play important roles in lipid biogenesis (Rowland and Voeltz, 2012), as well as the homeostasis of the contacting organelles. Direct contact between ER and corresponding organelles could achieve efficient material exchange inside the cell. But, how the cell efficiently exchanges material with its external environment?

Here, we describe a tubular membrane structure that widely exists inside cells, extending from the plasma membrane (PM) to the cytosol. We show that these PM tubes are highly dynamic, and have unique kinetic properties. We further determined how these PM tubes expedite membrane exchange between the plasma membrane and contacting organelles, and how they facilitate receptor presentation. Both mechanisms contribute to efficient material exchange between the internal and the external environment of the cell.

Results

A widely existing tubular membrane structure inside cells

To visualize membrane dynamics, we labeled the plasma membrane by GFP C-terminally fused with a CAAX sequence from H-Ras (Homo sapiens NP_005334.1, amino acid 170-189). We noticed fluorescent signal from the cell surface as well as some internal structures. Interestingly, besides spheres which we believe were previously reported as trafficking vesicles, GFP-CAAX labeled internal structures also include tubular structures (Figure 1A,1C). These GFP-CAAX labeled tubular membrane structure (tubes for short), are lying underneath the plasma membrane, spanning from one side of a cell to the other side, or from the center to the edge of a cell (Figure 1A-1D). In addition, the tubes were observed in cells with the plasma membrane labeled by fluorescent proteins fused with tetraspanin family proteins (CD9 in Figure 4A).

To ascertain whether the tubes observed are caused by the expression of fluorescent protein fusions, we used live-cell imaging to monitor dye-labeled membrane structures in real time. PKH26 is a widely used lipophilic dye and labels biological membrane by inserting its long aliphatic tails into the lipid regions of the membrane. The length of PKH26 labeled tubular structures had similar distribution as

98 GFP-CAAX labeled tubes (Figure 1F). Additional experiments demonstrated that
99 GFP-CAAX and PKH26 labeled the same tubes (Figure 1G). In summary, using
100 either fluorescent protein fusions or fluorescent lipid, we discovered a novel tubular
101 structure that widely exists inside cells.

102 We first discovered the tubes in HeLa cells. Then we confirmed that they
103 could be observed in a variety of commonly used cell lines, including 293FT, COS7,
104 NIH/3T3, Raw 264.7, MDCK, NRK and HT-1080 (data not shown). Strikingly, these
105 tubes seemed to be stable through the cell cycle (Figure 1H). When a cell divides,
106 the plasma membrane undergoes dramatic reformation. However, the tubes persist
107 and exist in dividing cells (Figure 1I).

108 Limited literature searching suggests that at least in developing worm embryo
109 (8-cell stage, Chen et al., 2014) and zebrafish larva (notochord sheath cells, 7-day
110 post fertilization, Dale and Topczewski, 2011), there are tubular membrane structures
111 in animals expressing fluorescent protein at the plasma membrane. We confirmed
112 the second in Figure 1J.

113 Recent advances in super-resolution microscopy have substantially increased
114 the spatial resolution. We then performed live-cell analysis using a super-resolution
115 microscopy, Airyscan from ZEISS (Figure 2A). The diameter of the tubes (labeled by
116 mMaple3-CAAX) was measured to be 253 ± 49 nm (mean ± standard deviation,
117 Figure 2E). Both ends of a tube spanning across a cell are shown, with one end
118 residing closely to the plasma membrane (Figure 2B).

119 Using a combination of paraformaldehyde and glutaraldehyde reagents, we
120 were able to fix the tubes for N-STORM super-resolution imaging (Figure 2C). We
121 measured the diameter of the tubes (labeled by mMaple3-CAAX) to be 224 ± 60 nm
122 (mean ± standard deviation, Figure 2E). With N-STORM, we were able to observe
123 the hollow structure of the tubes in some cross sections (Figure 2D). Notably,
124 previously smooth tubes bulged to form a lot of membrane bubbles. We think that
125 bulging may be due to an un-synchronized fixation of the fast flowing tubular
126 membrane.

127 Tubular membrane structures have openings on the plasma 128 membrane

129 Inspired by the hollow structure, we were curious whether we could mark the tubes
130 by what they transport. Dextran is a complex branched polysaccharide, taken by cells
131 via endocytosis, and is used as a classical marker for membrane vesicle trafficking.
132 We added fluorescent dextran (10,000 MW) into the cell culture media and pulsed for
133 15 min, then chased with plain culture media and imaged the living cells. Consistent
134 with previous knowledge that dextran is taken and transported as vesicles, we
135 observed that most fluorescent signals were vesicles of various sizes (data not
136 shown). Moreover, we were able to find tubular structures with bright fluorescence.
137 By using a fluorescent dextran with a large molecule weight (500,000 MW) and
138 reducing the pulse time to 5 min, most of the dextran signals were limited to tubular
139 structures (Figure 2G). Furthermore, fluorescent dextran also marked the tubes
140 labeled by RFP-CAAX. Thus, we show that the tubes inside cells with the hollow
141 structure may participate in dextran transport.

142 After careful examination of fluorescent dextran marked tubes, we noticed
143 several interesting features. Only some portions of GFP-CAAX labeled tubes were
144 marked with fluorescent dextran, while all fluorescent dextran marked tubular
145 structures were labeled by GFP-CAAX. Every dextran marked tube had at least one
146 end very close to the plasma membrane. Furthermore, the end close to the plasma
147 membrane always had a stronger fluorescent signal compared with the other end.
148 Based on these features, we hypothesized that dextran was siphoned into the tube
149 due to its opening on the plasma membrane.

150 To test our hypothesis, we added fluorescent dextran (70,000 MW) into the
151 cell culture media for only 10 sec before fixation. Strikingly, fluorescent dextran
152 siphoned in and vividly marked tubular structures spanning across the cell (Figure
153 2K,2L), with enriched signals from fixation generated bulged membrane bubbles
154 (Figure 2H).

155 We measured the average diameter of the tubes to be 224~253 nm, and thus
156 dextran with a comparable diameter would not be able to siphon in and mark the
157 tubes. We incubated cells with different sized fluorescent dextran (10,000 MW,
158 30,000 MW, 70,000 MW, 500,000 MW, 2,000,000 MW), and measured the labeling
159 efficiency (Figure 2I,2J). Because the concentration of fluorescent dextran we used
160 was 2 mg/ml, the change of fluid viscosity upon the addition of dextran was minimal
161 and could be neglected. While dextran with a molecule weight less than 70,000
162 siphoned into the tubes and marked over 80% length of the structures, dextran

163 2,000,000 MW could not mark any internal cellular structure. Respectively, the
164 Stokes radius of 57 KD and 157 KD dextran are 5.5 nm and 9.1 nm (Peters, 1984).
165 Together, we showed that these widely existing tubes have openings on the plasma
166 membrane.

167 Inward tubulation of the plasma membrane

168 To confirm a direct connection between the plasma membrane and the tubes, we
169 photo-converted a portion of the membrane from green fluorescence to red in cells
170 expressing mMaple3-CAAX (Wang et al., 2014), and performed live-cell imaging of
171 converted membrane. A red tube initiated from a region with no visible vesicle or
172 organelle, and protruded into a non-illuminated region (Figure 3G), suggesting that
173 the tubes were built using the material from the initiation plasma membrane. This is
174 consistent with the observation that the tubes have openings on the plasma
175 membrane. In addition, upon green-to-red conversion, previously existing tubes
176 immediately obtain red signals, indicating a fast membrane flow on the tubes.

177 To measure the directionality of the tubular membrane flow, we performed
178 fluorescence recovery after photo-bleaching (FRAP) analysis (Figure 3E-F). Due to
179 the fast membrane flow, fluorescence of all measured regions decreased upon
180 bleaching. During the recovery phase, within a limited time, only one side of the
181 bleached region showed increased fluorescence. The estimated membrane flow
182 speed (2~3 μm in 6 sec) is consistent with calculated fast protrusion speed (32.3
183 μm/min, Figure 3D) of the tubes. Thus, we conclude that the membrane flow on the
184 tubes is unidirectional.

185 Careful examination of live-cell imaging data revealed further evidence
186 supporting the direct connection between the plasma membrane and the tubes.
187 There are tubes retracting from the plasma membrane (Figure 3H). There are tubes
188 protruding and connecting to the plasma membrane (Figure 3H,3I). And tubes
189 initiating from the plasma membrane (Figure 3J). Infrequently, there were tubes
190 connecting to the plasma membrane and supporting filopodia outgrowth (Figure 3K).
191 Together, we discovered that inward tubulation of the plasma membrane forms tubes
192 spanning across the cell.

193 Plasma membrane tubes are not tubular mitochondria or tubular
194 endoplasmic reticulum

195 Mitochondria, found in most eukaryotic cells, play an important role in energy
196 production. Recent data indicate that besides fission and fusion, dynamic tubulation
197 of mitochondria is an essential mechanism for its network formation (Wang et al.,
198 2015). To clarify that the plasma membrane (PM) tubes are not tubular mitochondria,
199 we labeled mitochondria with a fluorescent protein (FP) fused with the C terminus of
200 ActA, and labeled PM tubes with FP-CAAX. With FP swapping combination, in
201 neither case, the tubes colocalize with mitochondria (Figure 4C).

202 The endoplasmic reticulum (ER) is critical for both protein and lipid synthesis
203 in eukaryotic cells. ER is a network of tubes and sheets (Voeltz and Prinz, 2007;
204 Voeltz et al., 2006). To clarify that the PM tubes are not tubular ER, we labeled ER
205 with GFP fused with various ER residing proteins (calreticulin, ERD-2-like protein 1,
206 Sec61b, reticulon 4a) or a KDEL sequence. In none of the cases, the PM tubes
207 overlapped with any ER structure (Figure 4D). Even though the tubular ER spread,
208 extended and covered almost all the cytoplasmic space, PM tubes always stayed out
209 of the ER territory.

210 To further confirm that there is no interaction between PM tubes and ER, we
211 shifted the balance between tubular ER and ER sheets. As previously reported, when
212 CLIMP-63 was over-expressed in cells, the percentage of tubular ER decreased
213 (Klopfenstein et al., 2001), while overexpressing ATL1(K80A) increased long and
214 unbranched ER tubules (Hu et al., 2009), (Figure 4E-F). In both cases, neither the
215 length of PM tubes nor the number of tubes in the cell changed (Figure 4F').
216 Together, we conclude that PM tubes are not tubular ER nor mitochondria.

217 Plasma membrane tubes transiently interact with the Golgi 218 apparatus

219 We showed that the plasma membrane inward tubulated into the cell, and maintained
220 openings on the plasma membrane. We were curious where the other ends of these
221 tubes reside. Using a panel of well-characterized markers for intracellular organelles,
222 we performed colocalization analysis. Although small portions of Rab5a/Rab5b
223 positive early endosomes aligned along the tunnels, we failed to detect any
224 connection between the ends of PM tubes with autophagosomes, peroxisomes,
225 lysosomes, early or late endosomes (Figure 4G).

226 The Golgi apparatus processes and packages cargos into vesicles before
227 delivering them to their targets. If the tubes involved in delivering cargos, it is likely
228 that they cease at the Golgi apparatus. We labeled the Golgi apparatus either by
229 expressing GFP fused with Golgi residing proteins (β1,4-galactosidase,
230 sialyltransferase; data not shown), or by immunofluorescence using an antibody
231 against GM130 (*cis*-Golgi marker). In cells with both the tubes and the Golgi labeled,
232 the intracellular ends of the tubes somewhat overlapped with the Golgi. However,
233 using dual-color live-cell imaging, we could not ascertain whether or not the tubes
234 protruding from the plasma membrane interact with the Golgi apparatus.

235 To confirm the potentially transient interaction between the Golgi and PM
236 tubes, we employed the SunTag fluorescence tagging strategy (Tanenbaum et al.,
237 2014; Yao et al., 2017). In cells only expressing GCN4-sfGFP-GB1-CAAX
238 (^{SunTag}CAAX, GCN4 is a single-chain variable fragment antibody against V4 peptide),
239 both the plasma membrane and the tubes, as well as trafficking vesicles, were
240 labeled by GFP-CAAX. In control cells expressing GCN4-sfGFP-GB1 (^{SunTag}cyto) and
241 an array of 10 copies of V4 peptide fused with sialyltransferase (SiT-10xV4),
242 fluorescence was cytoplasmic and no membranous structure was labeled (data not
243 shown), consistent with the finding that 10xV4 part of SiT-10xV4 is non-cytoplasmic.
244 Interestingly, in cells expressing ^{SunTag}CAAX and SiT-10xV4, neither the plasma
245 membrane nor most of the tubes were labeled, but the Golgi was labeled. It seemed
246 that the ^{SunTag}CAAX signal was sequestered in the Golgi apparatus. Notably, the
247 SunTag part of ^{SunTag}CAAX is cytoplasmic as of ^{SunTag}cyto, with the difference that
248 ^{SunTag}CAAX resides on the plasma membrane, or on the cytosolic surface of ER and
249 Golgi during its maturation (Apolloni et al., 2000; Choy et al., 1999). These data
250 suggested that the plasma membrane continuously has transient interaction with the
251 Golgi apparatus through the tubes, and this interaction provides membrane continuity
252 and must surpass the topological barrier.

253 Post-Golgi carriers are important components of intracellular transport, and
254 some of the post-Golgi carriers are membrane tubules being pulled out of the *trans*-
255 Golgi network (Almeida et al., 2011; Kreitzer et al., 2003; Luini et al., 2008; Russo et
256 al., 2016). To ascertain that the PM tubes are not post-Golgi tubules, we used dual-
257 color live-cell imaging to compare the dynamics of Rab1a labeled post-Golgi tubules,
258 and RFP-CAAX labeled PM tubes in real time. In summary, although the PM tubes
259 transiently interact with the Golgi, they are not post-Golgi tubules.

Actin filaments stabilize plasma membrane tubes

PM tubes are dynamic membrane structures, protruding and retracting all the time (Figure 3C). Other known intercellular structures with analogical dynamics are actin filaments and microtubules (Fletcher and Mullins, 2010). We postulated that some cytoskeletal filaments play important roles in regulating the dynamics of the tubes.

First, we labeled the actin filaments with LifeAct-RFP and performed colocalization analysis with GFP-CAAX labeled PM tubes. Although spatially some actin filaments extensively colocalize with some PM tubes (Figure 5B), their colocalization has a temporal difference. In protrusions, PM tubes always precede actin filaments elongation (Figure 5A,5C-D). In retractions, the actin filaments have to disappear prior to the tubes (Figure 5C-D).

Second, we used a panel of small molecules inhibitors to perturb the actin dynamics in the cells. When the actin assembly was inhibited by latrunculin B treatment (Figure 5E), PM tubes still protruded, suggesting that the actin filaments do not initiate the elongation of the tubes. In addition, either cytochalasin D or latrunculin B treatment reduced the length of the tubes and the number of PM tubes in the cell. Thus, actin assembly does not initiate but stabilize PM tubes.

Microtubule dynamics drives plasma membrane tubes

To test the role of microtubules in regulating the dynamics of PM tubes, we performed colocalization analysis with RFP-CAAX labeled tubes and α-tubulin-GFP labeled microtubules (Figure 5G). Colocalization of both fluorescent signals suggested a strong connection between PM tubes and microtubules.

Nocodazole and paclitaxel are two chemical inhibitors that affect microtubule dynamics differently. While nocodazole interferes the assembly and accelerates the disassembly of microtubules, paclitaxel stabilizes the existing filaments and promotes microtubule assembly. In cells treated with nocodazole for 30 min, microtubules were completely disassembled, and the number of protruding PM tubes significantly decreased. However, the tubes persist (Figure 5H). It is consistent with previous observations that actin filaments stabilize the tubes.

289 In cells treated with paclitaxel for 30 min, we still observed rapid PM tube
290 elongation suggesting microtubule polymerization is not the driving mechanism for
291 PM tubulation, although calculated microtubule polymerization speed is 30 μm/min
292 (Parsons and Salmon, 1997), a close match to our measured tube fast protrusion
293 speed (32.3 μm/min).

294 To confirm the elongation of PM tubes does not interact with the plus ends of
295 microtubules, we labeled the plus ends of microtubules with EB1-GFP and examined
296 where the ends of RFP-CAAX labeled PM tubes reside. The plus ends of
297 microtubules were observed as comets, and these EB1-GFP positive comets move
298 quickly from the center to the periphery. However, the ends of the PM tubes didn't
299 overlap with any EB1-GFP signal (Figure 5I). Besides, it is difficult to image how
300 inward tubulated plasma membrane interacts with known microtubule tip attachment
301 complexes (Allan and Vale, 1994; Allan and Vale, 1991; Waterman-Storer et al.,
302 1995). Together, our results indicate that PM tubes elongate along microtubules, by
303 interacting with microtubule side-binding proteins.

304 Non-dynamic plasma membrane tubes are enriched with 305 cholesterol

306 We were curious how the PM tubes remain their shape without stabilizing actin
307 filaments. Cholesterol is a lipid essential for cell viability that plays a critical role in
308 maintaining membrane integrity and is always found in rigid membrane subdomains
309 (Simons and Toomre, 2000). We treated cells with methyl-beta-cyclodextrin (MβCD)
310 to deplete plasma membrane cholesterol. Interestingly, in the cells depleted of
311 cholesterol, the PM tubes were very similar to the ones after cytochalasin D, or
312 latrunculin B treatment (data not shown), suggesting cholesterol stabilizes PM tubes.

313 Then, we fixed and stained cells with filipin, a fluorescent compound that
314 specifically binds to cholesterol and is widely used as a histochemical marker for
315 cholesterol. We observed labeling of filipin on some PM tubes (Figure 5J-K). Only
316 small portions of PM tubes have partial filipin labeling, suggesting loading cholesterol
317 to a PM tube is a rapid process.

318 Furthermore, we performed live-cell imaging of cells incubated with a
319 fluorescent cholesterol analog, dehydroergosterol (DHE). We found that the PM
320 tubes were labeled by DHE (Figure 5L), and those non-dynamic tubes had strong

321 DHE labeling. High concentration of cholesterol in membrane lipid results in reduced
322 membrane fluidity. Our results demonstrated that cholesterol plays a role in
323 stabilizing the PM tubes.

324 Plasma membrane tubes expedite membrane exchange with the 325 endoplasmic reticulum

326 Although we have shown that PM tubes are not tubular ER, we wondered whether
327 these two different membrane structures interact with each other. Recent data
328 indicate that extended synaptotagmin protein 1 (E-Syt1), an ER protein, bridges ER
329 and PM upon increased cytoplasmic calcium concentration (Giordano et al., 2013).
330 These ER-PM contact sites were suggested to facilitate direct lipid transfer between
331 membranes (Fernandez-Busnadiego et al., 2015; Schauder et al., 2014). We
332 performed live-cell imaging of cells expressing RFP-CAAX and GFP–E-Syt1. In
333 unstimulated cells, E-Syt1 was exclusively located on the ER network. Then, we
334 treated cells with thapsigargin (Tg), a non-competitive inhibitor of the ER calcium-
335 ATPase pump, to induce calcium release from the ER. Strikingly, with the increase of
336 cytoplasmic calcium, E-Syt1 relocalized to the PM tubes and brought the ER to be in
337 close contact with the PM tubes. 20-sec Tg treatment was sufficient to induce ER-PM
338 contact sites, preferably on PM tubes (Figure 6A-B,6H), without affecting ER
339 morphology (Figure 6C-D). Similarly, some E-Syt3 marked ER-PM contact sites
340 formed on the PM tubes (Figure 6E,6H). In summary, the E-Syt1 and E-Syt3 marked
341 ER-PM contact sites preferably formed on the PM tubes, which were tubular
342 structures extending from the plasma membrane.

343 Plasma membrane tubes facilitate the surface presentation of 344 receptors

345 Enlightened by the shortcut that the cell has taken to form the ER-PM contact sites,
346 we wondered whether the PM tubes were the preferred plasma membrane
347 subdomains where receptors were being targeted for presentation.

348 Glucose is the optimal fuel for most living cells. Uptake of glucose into
349 mammalian cells is mediated mainly by the glucose transporters as the biological
350 membrane is impermeable to glucose. GLUT1 was the first cloned glucose
351 transporter (Mueckler et al., 1985), and widely exists in all types of cells.

352 Immunolocalization of endogenous proteins reveals that GLUT1 dots spread over the
353 plasma membrane (Figure 7A). To investigate the role of PM tubes in GLUT1 surface
354 presentation, we cultured the cells in glucose deprivation conditions for different
355 periods of time. Immediately after replenishing glucose, we fixed, immunostained and
356 examined the localization of endogenous GLUT1. As expected, under glucose
357 deprivation, increased GLUT1 is required on the plasma membrane. These on-
358 demand GLUT1 first enriched on PM tubes and then spread over the plasma
359 membrane (Figure 7B-D). Similarly, after replenishing glucose, the rapid clearing of
360 GLUT1 from the PM tubes preceded the decrease of GLUT1 from the plasma
361 membrane.

362 Thus, we demonstrated that the PM tubes were used to facilitate GLUT1
363 surface presentation in changing environments. However, we could not observe
364 similar behavior for EGFR (Figure 7G-H), a receptor tyrosine kinase, with its major
365 role in signaling transduction.

366 Discussion

367 Here, we reported that the plasma membrane (PM) extends tubular structures into
368 the cytoplasm in cells. Inward tubulation of PM provides a shortcut for intercellular
369 compartments to interact with the external environment and expedites membrane
370 exchange between compartments.

371 Previously characterized tubular membrane structures

372 Using colocalization analysis, we showed that these PM tubes were previously
373 uncharacterized membrane structures. Below, we briefly summarize some of the
374 known ones.

375 ***Cilia:*** Ciliary membrane protrudes from PM, which is topologically opposite to
376 the PM tubes. While organized microtubule structures drive ciliary membrane
377 formation, PM tubes can protrude without either actin filaments or microtubules.
378 Functionally, cilia sense and transduce signaling by proteins enriched on the ciliary
379 membrane (Ishikawa and Marshall, 2011). Our initial characterization suggested that
380 the PM tubes expedite membrane exchange and receptor presentation. We believe
381 future studies around PM tubes would be inspired by the existing investigations about
382 the biogenesis and functions of cilia.

383 ***Tubular endoplasmic reticulum (ER):*** ER is where secreted and membrane
384 proteins are synthesized, and a major place for lipid manufacturing. ER is a
385 continuous membrane structure with a single lumen, which consists of tubes and
386 sheets. Rather than being pulled out by motors, studies have shown that reticulons
387 and their interacting proteins are the structure components shaping the tubular ER
388 (Hu et al., 2009; Voeltz et al., 2006). In yeast cells, cortical ER sheets would provide
389 extensive interaction between ER and PM (Manford et al., 2012). However, in cells,
390 the majority of ER sheets resides in perinuclear regions. We think that PM tubulation
391 would provide increased opportunities for ER to interact with PM by interactions
392 either between tubular ER and PM tubes, or between perinuclear ER sheets and
393 extended PM tubes.

394 ***Post-Golgi tubes:*** The Golgi apparatus is where proteins are post-
395 translationally modified and sorted for transport to their destinations. Many trafficking
396 events happen in post-Golgi compartments. Using either GFP chimeras or a
397 temperature sensitive form of the glycoprotein G of the vesicular stomatitis virus
398 (VSV-G), studies have shown that there are tubular structures, which are Rab1
399 positive, being pulled along microtubules and detached from Golgi cisternae
400 (Gallione and Rose, 1985; Presley et al., 1997; Russo et al., 2016). Post-Golgi tubes
401 are one of the diverse ways that cells use to transport cargos to the cell periphery
402 (Almeida et al., 2011; Anitei et al., 2010; Cooper et al., 1990; Feng et al., 2004;
403 Ganley et al., 2008; Kreitzer et al., 2003; Lippincott-Schwartz et al., 1990;
404 Pantazopoulou et al., 2014; Polishchuk et al., 2003; Raa et al., 2009; Sabharanjak et
405 al., 2002; Sciaky et al., 1997; Sherer et al., 2003; Wagner et al., 1994; Waguri et al.,
406 2003). The PM tubes characterized here display more rigid motion than post-Golgi
407 tubes. We have shown that a small number of PM tubes could interact with the Golgi
408 apparatus, and future investigation will be focused on when and how PM tubes
409 connect with Golgi.

410 ***Elongated endosomes:*** In the 1990s, tubular endosomal network has been
411 reported by two groups, after loading the cells with horseradish peroxidase for 30 min
412 and observed through electron microscope (Tooze and Hollinshead, 1991, 1992), or
413 after loading the cells with Texas red labelled transferrin for 60 min and observed
414 through low light video recording (Hopkins et al., 1990). Both studies suggested a
415 great continuity within endocytic pathways. Recently, when investigating the role of
416 ER in endosome fission, it was shown that cells treated with dynasore or depleted of
417 dynamin 2 by RNAi had Rab5 positive elongated endosomes (Rowland and Voeltz,

418 2012). Endosomes, formed by endocytosis (Antonescu et al., 2010; Howes et al.,
419 2010), are membrane structures that internalize proteins, lipids, *etc*. All these
420 elongated endosomes are topologically similar to PM tubes and have identical
421 membrane source - the plasma membrane. However, PM tubes are Rab5a/b
422 negative, transferrin receptor negative (data not shown), and some of them are
423 stable through the cell cycle. It requires further investigation to compare the
424 biogenesis of these two tubular structures. Also, there is Rab8-positive tubular
425 structures that form after macropinocytosis and mediate membrane recycling and
426 protrusion formation (Hattula et al., 2006; Roland et al., 2007). However, these Rab8-
427 positive tubules are sensitive to nocodazole and cytochalasin D treatment, while PM
428 tubes are not. Even though we have shown that the PM tubes connect with the
429 plasma membrane, little is known as to where they connect. Eisosome-like domains
430 in mammalian cells would be the first type of PM domains that we would investigate
431 in the future (Moreira et al., 2009; Walther et al., 2006). Since dynamic tubes lack
432 cholesterol, it is unlikely that PM tubes initiate from lipid rafts. On the contrary,
433 existing PM tubes are likely to connect with cholesterol lipid rafts to stabilize and
434 maintain themselves.

435 ***Mitochondrial and auto-lysosomal tubes:*** Tubulation of mitochondria and
436 auto-lysosomes is critical in maintaining organelle homeostasis (Reyes et al., 2011;
437 Swanson et al., 1987). Recent studies using *in vitro* reconstitution demonstrated that
438 a kinesin motor protein, Kif5B, decorates and pulls the mitochondrial outer
439 membrane, or the auto-lysosomal membrane, to form tubular structures (Du et al.,
440 2016; Wang et al., 2015). Kif5B travels along microtubules at an average speed of
441 49~54 μm/min (Nishiyama et al., 2002; Schnitzer et al., 2000), which is comparable
442 with the fast protrusion speed, providing one mechanism for PM tubulation. However,
443 the frequent transmission-switching-like protrusion dynamics, as well as the ability to
444 extend without polymerized microtubules, suggests a complex regulation that
445 involves in PM tubulation. Future studies will focus on finding the molecular machines
446 that are employed and comparing the difference between microtubule based and
447 actin filament based dynamics. For each PM tube, transmission-switching-like
448 protrusion suggests a smooth transition from microtubule-based to actin-filament
449 based dynamics, which must involve additional coordination between the two distinct
450 cytoskeleton networks.

451 In addition to the ones summarized above, in *Drosophila* respiratory system,
452 tracheoles invade into insect flight muscle T-tubules to form close contacts with every

453 mitochondrion (Peterson and Krasnow, 2015), providing an excellent example on
454 how physiological needs are met by extravagant membrane deformation.

455 The tunneling process

456 Virginia Woolf, an English writer in the twentieth century, used '*tunnelling process*' to
457 portray her characters' state of mind. She brought a character's past into the present
458 moment through his memory. She described this method of writing as '*dig[ging] out*
459 *beautiful caves*', and she thought it gives '*humanity, humour, depth*'. Woolf's tunnel
460 implies the possibility of coming and going between the past and the present.

461 We demonstrated that the cell uses inward tubulation of PM to bring the
462 external environment close to its intercellular compartments. Cellular organelles are
463 like Woolf's caves, having their glory moments, and more importantly, organelles
464 shall connect, precisely and efficiently.

465 We propose to name the tubular membrane structures described here as the
466 plasma membrane tunnels (PM tunnels), and name this phenomenon membrane
467 tunneling.

468 The PM tunnels are distinct from previously reported nanotubules that exist
469 between identical organelles or cells. Stroma-filled tubules are formed by tubulation
470 of the inner and outer plastid membranes. They connect and transfer
471 macromolecules between plastids (Kwok and Hanson, 2004; Natesan et al., 2005).
472 To pass through plant cell wall, plasmodesmata are used. Within plasmodesmata,
473 there are desmotubules connecting the ER of adjacent cells (Zambryski, 1995).
474 Between mammalian cells, nanotubules form complex networks and transfer
475 endosomal structures between cells (Rustom et al., 2004). Within mammalian cells,
476 both short-lived and long-lasting mitochondrial nanotubules have been described,
477 which are suggested to be important for cardiomyocyte function (Huang et al., 2013).
478 To enable bacterial social behaviors, nanotubular superhighways directly exchange
479 cytoplasmic factors between *B. subtilis* cells (Dubey and Ben-Yehuda, 2011).
480 Although some of the nanotubules mentioned above bear the name of "tunneling
481 nanotubules", the emphasis of membrane tunneling phenomenon proposed here is
482 not limited to the shape of the structure, but also the active process to achieve
483 membrane exchange.

484 **Membrane tunneling is a general adaptation to compartmentalized**
485 **cellular biology**

486 Compartmentalized cellular biology reflects the principle that a eukaryotic cell uses to
487 organize its internal landscape. Because of the compartmentalization, how to
488 exchange material precisely and efficiently between different compartments is the
489 utmost important matter a cell must deal with.

490 Previous studies have revealed that the cell uses membrane vesicle
491 trafficking to precisely exchange material. Here, we described a second approach,
492 membrane tunneling, which the cell uses to accelerate material exchange, and we
493 provide evidence that the plasma membrane tunneling expedites membrane
494 exchange and receptor presentation. Both membrane vesicle trafficking and
495 membrane tunneling achieve material exchange, probably with the first being
496 specialized in cargo delivery and the second in membrane exchange. Both
497 approaches are probably a universal adaptation to compartmentalized cellular
498 biology.

499 Experimental procedures

500 Reagents and Materials

501 Commercial antibodies were obtained from BD Biosciences (GM130, cat# 610822),
502 Abcam (GLUT1, cat#115730) and Sino Biological (EGFR, cat# 1001-MM08), and
503 Jackson Immuno Research (Alexa Flour 647 conjugated secondary antibodies).
504 Latrunculin B from Calbiochem, thapsigargin from Sigma, nocodazole from Selleck,
505 and paclitaxel from LC Laboratories. All other materials were from Sangon unless
506 otherwise indicated. Cells were obtained from ATCC, or gifts from collaborating
507 laboratories.

508 Cell culture, transient transfection and viral transduction

509 HeLa cells were cultured in DMEM supplemented with 10% FBS (HyClone), 100
510 U/ml penicillin, 100 μg/ml streptomycin and 1x GlutaMax (Gibco). Transient
511 transfections were performed using Lipofectamine 2000 (Invitrogen) and Opti-MEM
512 (Gibco), with reduced reagent incubation time. Viral packaging, infection and

513 fluorescence-activated cell sorting (FACS) were as described (Cai et al., 2008; Cai et
514 al., 2007).

515 Constructs and molecular cloning

516 PCR and subcloning were performed using standard methods. Most green
517 fluorescent protein (GFP) fusions were mEmerald based. Red fluorescent protein
518 (RFP) fusions were based on TagRFP-T, mApple or mCherry. Detailed primer
519 sequences are available upon request. To convert ^{SunTag}cyto into ^{SunTag}CAAX, primers
520 5-CCC tctaga acctacaagctgatcctgaacg-3 and 5-gac AAGCTTa
521 ggagagcacacacttgcagctcatgcagccggggccactctcatcaggag ggttcagctt CTC GGT CAC
522 GGT GAAG-3 were used to obtain GB1-CAAX, and PCR products were cut by XbaI
523 and HindIII, and ligated into ^{SunTag}cyto to replace its GB1. All constructs were verified
524 by Sanger sequencing.

525 Dextran loading assay

526 HeLa cells were transfected with indicated constructs, or made stably expressing
527 lines via viral transduction and FACS. The cells were plated onto glass bottom dishes
528 coated with 10 μg/ml fibronectin (EMD Millipore), and allowed to grow for 12 hr. We
529 incubated the cells with culture media containing 2mg/ml fluorescent dextran
530 (Molecular Probes, lysine fixable dextran: Texas Red, 3,000 MW, D3328; Texas Red,
531 10,000 MW, D1863; Texas Red, 70,000 MW, D1864; Fluorescein, 500,000 MW,
532 D7136; Fluorescein, 2,000,000 MW, D7137) for 10 sec, suck out the media and fixed
533 the cells with 4% paraformaldehyde and 0.5% glutaraldehyde in Kreb's S Buffer (145
534 mM NaCl, 5 mM KCl, 1.2 mM $CaCl_2$, 1.3 mM $MgCl_2$, 1.2 mM NaH_2PO_4, 10 mM
535 glucose, 20 mM HEPES pH 7.4 and 0.4 M sucrose) for 10 min. After three sequential
536 washes by PBS, the samples were immunostained (Cai et al., 2007) and imaged.

537 Light microscopy and statistical analysis

538 Images, unless otherwise indicated, were captured using a spinning disk confocal
539 scan head (CSU-X/M2N, Yokogawa) attached to an inverted microscope (IX-81,
540 Olympus) and an EMCCD camera (pixel size = 16.016 μm; DU897BV, Andor) and
541 controlled by Micro-Manager software. For most of the imaging, 150XOTIRF
542 objective (N.A. = 1.45, airy disk radius = 210.3 nm) was used. To image zebrafish
543 animal, 60XS objective (N.A. = 1.3, airy disk radius = 234.6 nm) was used.

544 The GFP and RFP were excited by 488-nm and 561-nm lasers. The emissions were
545 separated by FF410/504/582/669-Di01 and further passed emission filters FF02-
546 510/10 (mEmerald), FF01-590/20 (mApple), FF01-583/22 (TagRFP-T), FF01-615/20
547 (mCherry), respectively. Alignment of the GFP and RFP channels was roughly tuned
548 with 100-nm fluorescent microspheres (TetraSpeck). Filipin and DHE imaging were
549 performed as previously described (Hao et al., 2002; Mesmin et al., 2011).
550 Kymograph analysis was based on timelapse movies as described in the figure
551 legends. Statistical analyses were performed using Prism (Graphpad). All
552 experiments were independently performed in triplicate, with at least 5 cells analyzed
553 in each, resulting N>15; unless otherwise indicated. Representative images are
554 shown.

555 Author contributions

556 LFY, LZ and LC conceived and designed the experiments. LFY and LZ performed
557 experiments. LFY, LZ and LC analyzed the data. RZ did the experiments in
558 zebrafish. LC wrote the manuscript.

559 Acknowledgments

560 We acknowledge Tian-qi Chen for his intuitive questioning that leads to the initial
561 discovery; a lot of people for inspiring suggestions in the early stage of the
562 investigation; Hua Guo, Meng-yi Yao, Ling-hua Zhang and Wei Xu for critical
563 comments on this manuscript; Tsinghua Cytoskeleton Club members and 2016 Cell
564 Polarity Signaling GRC attendants for extensive discussions; Shu Mao for helping
565 Filipin and DHE imaging; Hexige Saiyin for suggestion on the GLUT-1 antibody;
566 Siyuan Wang and Xiaowei Zhuang for providing the mMaple3-vimentin plasmid,
567 Junjie Hu for providing reticulon 4a, atlastin-1(K80A) and CLIMP-63 plasmids, Yang
568 Chen and Li Yu for providing normal rat kidney epithelial cells (NRK), Xiang Zhao
569 and Su Guo for providing the *Tg*(*EF1a*: myr-Tdtomato) transgenic zebrafish line, Jie
570 Wang and Yangming Wang for providing the GCN4-sfGFP-GB1 plasmid, Xiao-li
571 Zhang for providing the EGFP-Rab1a, EGFP-Rab5a/5b, EGFP-Rab7a, LC3-EGFP,
572 EGFP-PXMP2 and LAMP1-TagRFP-T plasmids; Yujie Sun and Zhen Liu for
573 suggestions in analyzing STORM data; Bi-Chang Chen, Eric Betzig, Fengzhu Xiong
574 and Sean Megason for sharing high-resolution images of developing embryos; and
575 the assistance of microscopy application specialists from Nikon Instruments and

ZEISS. LC was supported by the National Natural Science Foundation of China grants (31222019 and 31271428), the Thousand Young Talents Plan and by funds from Fudan University and YZT Foundation.

579 # Figures

580 ## Figure 1. Widely existence of tubular membrane structures.

581 A- HeLa cells expressing GFP-CAAX were lively imaged by spinning disk confocal
582 microscopy (SDCM). Slices of a Z stack from optical sectioning are presented as
583 montage. Scale bar = 5 μm.

584 B- Slices from (A) were imported into Imaris (Bitplane), background subtracted,
585 smoothened using the default Gaussian filter, volume rendered and displayed.

586 C- The percentage of GFP-CAAX expressing HeLa cells with the tubular membrane
587 structures, presented as box and whisker plot (5-95 percentile).

588 D- For cells as in (C), the length of the tube was divided by the long cell axis, and the
589 percentage presented as box and whisker plot.

590 E- Schematic diagram of the tubular membrane structures we discovered (lines), with
591 circles representing membrane vesicles.

592 F- HeLa cells were trypsinized, stained with PKH26 dye, plated on fibronectin coated
593 glass bottom dishes, and lively imaged by SDCM. PKH26 labeled tubular structures
594 were quantified and presented as in (D).

595 G- HeLa cells expressing GFP-CAAX were stained and imaged as in (F). Yellow
596 arrowheads indicate a GFP-CAAX and PKH26 double positive tube. Quantification
597 on maximum intensity projections of Z stacks from optical sectioning shows 97.5 ±
598 9.3% GFP-CAAX tubes are PKH26 positive (mean ± standard deviation).

599 H- HeLa cells stably expressing GFP-CAAX were imaged by SDCM overnight. The
600 cell underwent cell division. Expanded views of yellow dash lines boxed regions are
601 displayed in the lower panels.

602 I- HeLa cells as in (H), slices of a Z stack from optical sectioning are presented.
603 Yellow arrowheads indicate the GFP-CAAX marked tubes. Gray arrow points to the
604 resulting cells after the division.

605 J- 7 dpf *Tg*(*EF1a*:myr-Tdtomato) zebrafish larva was anesthetized and embedded in
606 low melting agarose in lateral position. Notochord sheath cells were lively imaged by
607 SDCM. Maximum intensity projections of Z stacks are displayed, with expanded view
608 showing individual slices of yellow dash lines boxed regions. Yellow arrowheads
609 indicate the myr-Tdtomato marked tubes.

610

Figure 1

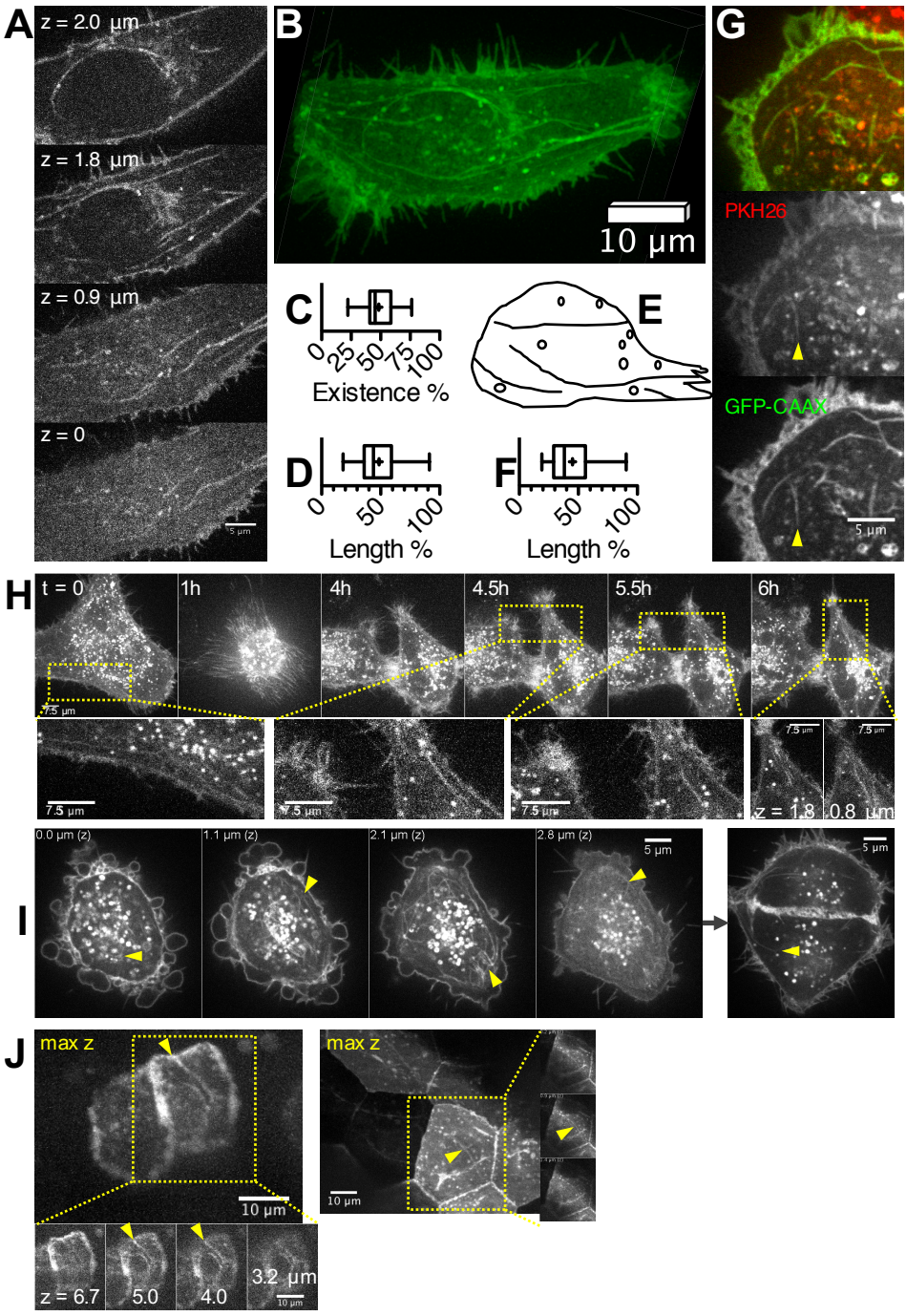
A
z = 2.0 µm
z = 1.8 µm
z = 0.9 µm
z = 0
B
10 µm
C
0 25 50 75 100
Existence %
E
D
0 50 100
Length %
F
0 50 100
Length %
G
PKH26
GFP-CAAX
5 µm
H
t = 0
1h
4h
4.5h
5.5h
6h
7.5 µm
z = 1.8 0.8 µm
I
0.0 µm (z)
1.1 µm (z)
2.1 µm (z)
2.8 µm (z)
5 µm
J
max z
10 µm
z = 6.7
5.0
4.0
3.2 µm

611 **Figure 2. Inward tubulation of the plasma membrane.**

612 A- HeLa cells expressing GFP-CAAX were lively imaged by the LSM 880 laser
613 scanning microscope with Airyscan (ZEISS). Slices of a Z stack from optical
614 sectioning are presented as montage. Scale bar = 5 μm.

615 B- Maximum intensity projection of an Airyscan Z stack from (A) is displayed on the
616 left, with expanded view of yellow dash line boxed region on the right. Two slices of
617 the Z stack presented with yellow arrowheads indicating the two ends of the tube.

618 C- HeLa cells expressing mMaple3-CAAX were fixed with 4% paraformaldehyde and
619 0.5% glutaraldehyde, and imaged by a N-STORM super-resolution microscope
620 (Nikon). Yellow dash line boxed region of the cell is displayed in expanded view.

621 D- Pixel intensities around the tubes were normalized and plotted based on their
622 distances to the axis. A detailed view of the distribution within 0.1 μm of the axis is
623 displayed in the upper panel. Grey lines were from 7 Airyscan captured tubes and
624 pink lines were from 7 N-STORM captured tubes.

625 E- Tube diameters were measured by the full-width-half-maximum (FWHM) method,
626 and presented as box and whisker plots (10-90 percentile) with the outliners.

627 F- Schematic diagram of dextran loading assay: the cells were plated on fibronectin
628 coated glass for 12 hr, and incubated with lysine-fixable fluorescent dextran
629 containing culture media.

630 G- HeLa cells expressing GFP-CAAX were treated as in (F) with 500,000 MW
631 dextran for 5 min, and lively imaged by SDCM.

632 H- HeLa cells expressing GFP-CAAX were treated as in (F) with 70,000 MW dextran
633 for 10 sec, fixed and imaged by Airyscan. Yellow arrowheads indicate dextran
634 containing membrane bubbles.

635 I- Fluorescent dextran with different molecular weights were used (KD, kilodalton).
636 HeLa cells expressing GFP-CAAX were treated as in (F) for 10 sec, fixed and
637 imaged by SDCM.

638 J- For cells as in (I), the length of the dextran loaded region was divided by the length
639 of the tube, and the percentage presented as box and whisker plots. * indicates that

640 the cells were incubated with 500,000 MW dextran for 1 min, while ** were incubated
641 with 2,000,000 MW dextran for 3 min.

642 K- Plain HeLa cells were treated as in (F) with 70,000 MW dextran for 10 sec, fixed,
643 imaged by SDLM, and presented as maximum intensity projection of a Z stack from
644 optical sectioning.

645 L- For cells as in (K), the length of the longest tube loaded with dextran was divided
646 by the long cell axis, and the percentage presented as scatter dot plot.

647

Figure 2

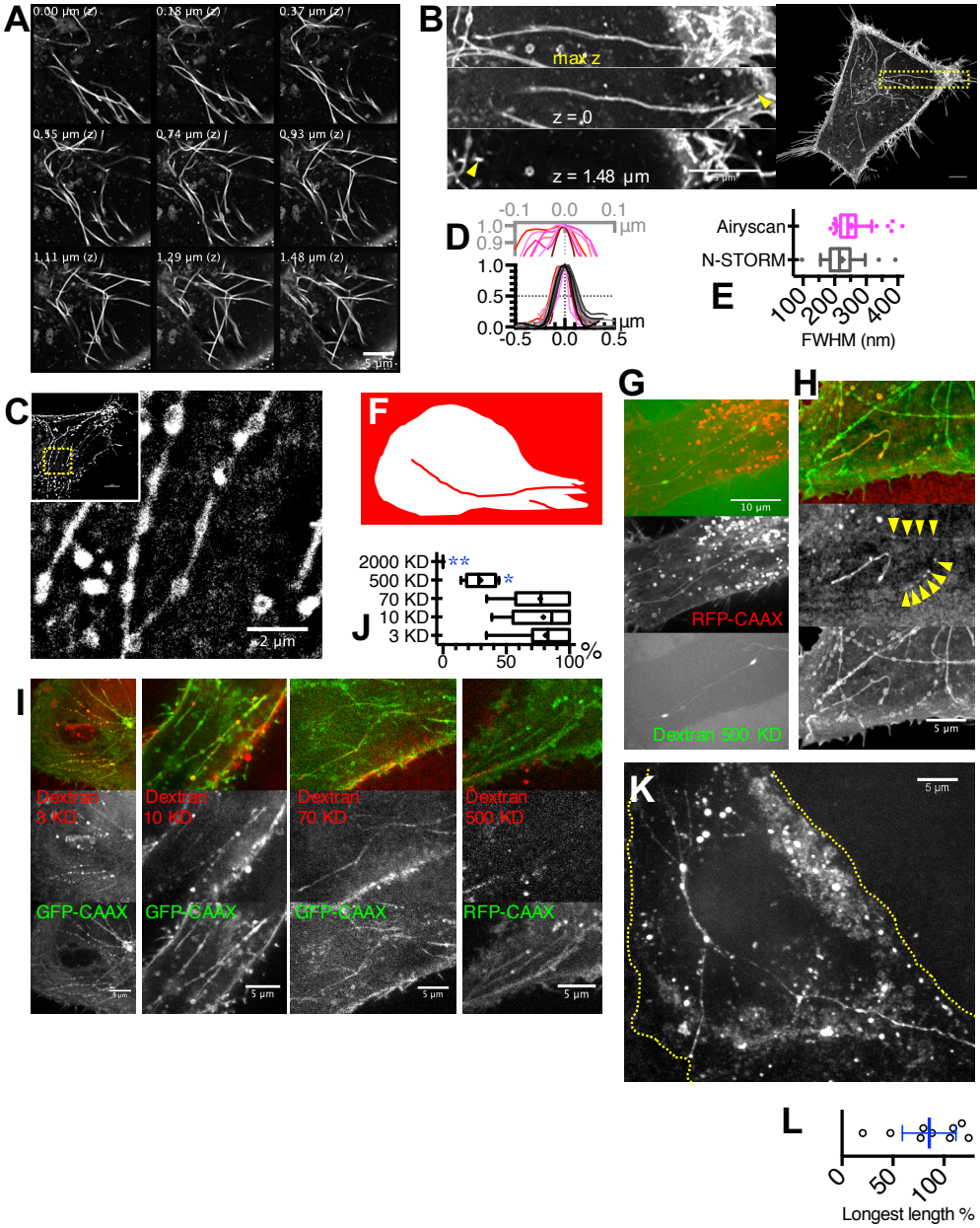
A
0.00 µm (z)
0.18 µm (z)
0.37 µm (z)
0.55 µm (z)
0.74 µm (z)
0.93 µm (z)
1.11 µm (z)
1.29 µm (z)
1.48 µm (z)
5 µm
B
max z
z = 0
z = 1.48 µm
D
-0.1
0.0
0.1
µm
1.0
0.9
0.5
0.0
-0.5
0.0
0.5
µm
Airyscan
N-STORM
E
100
200
300
400
FWHM (nm)
C
2 µm
F
2000 KD
500 KD
70 KD
10 KD
3 KD
J
0
50
100
%
G
10 µm
RFP-CAAX
Dextran 500 KD
H
5 µm
I
Dextran 3 KD
Dextran 10 KD
Dextran 70 KD
Dextran 500 KD
GFP-CAAX
GFP-CAAX
GFP-CAAX
RFP-CAAX
5 µm
K
5 µm
L
0
50
100
Longest length %

648 **Figure 3. Dynamics of the plasma membrane tubes.**

649 A- HeLa cells expressing GFP-CAAX were lively imaged by SDCM and presented as
650 timelapse montage. Yellow arrowheads indicate one end of a protruding tube. Scale
651 bar = 5 μm.

652 B- Kymograph of the protruding tube in (A). Horizontal line = 5 μm; vertical line = 1
653 min.

654 C- For cells as in (A), kymograph analysis as in (B) was used to calculate the
655 dynamic parameters, which were presented as box and whisker plots.

656 D- The protrusion speed of (C) presented in a histogram. Sum of two Gaussians was
657 fit to the data to calculate the means.

658 E,F- HeLa cells expressing GFP-CAAX were lively imaged by a laser scanning
659 microscope. The red dash line boxed region was photobleached. Pixel intensities of
660 different regions of the tube were plotted over time. Pink arrowhead indicates the
661 retracting tube.

662 G- HeLa cells expressing mMaple3-CAAX were lively imaged by SDCM. Yellow dash
663 line boxed region was illuminated with 405 nm laser for 1 sec to convert some green
664 fluorescent mMaple3-CAAX to red fluorescent mMaple3-CAAX. Images are
665 presented as timelapse montage. Yellow arrowheads indicate a tube that imitates
666 from the illuminated region and protrudes into the non-illuminated region.

667 H,I,J,K- HeLa cells expressing GFP-CAAX were lively imaged by SDCM and
668 presented as timelapse montage horizontally. In (H), slices of the Z stack from optical
669 sectioning at t = 140 sec are presented as montage vertically. Cyan arrowheads
670 indicate one end of a retracting tube, and yellow arrowheads indicate ends of
671 protruding tubes.

672

Figure 3

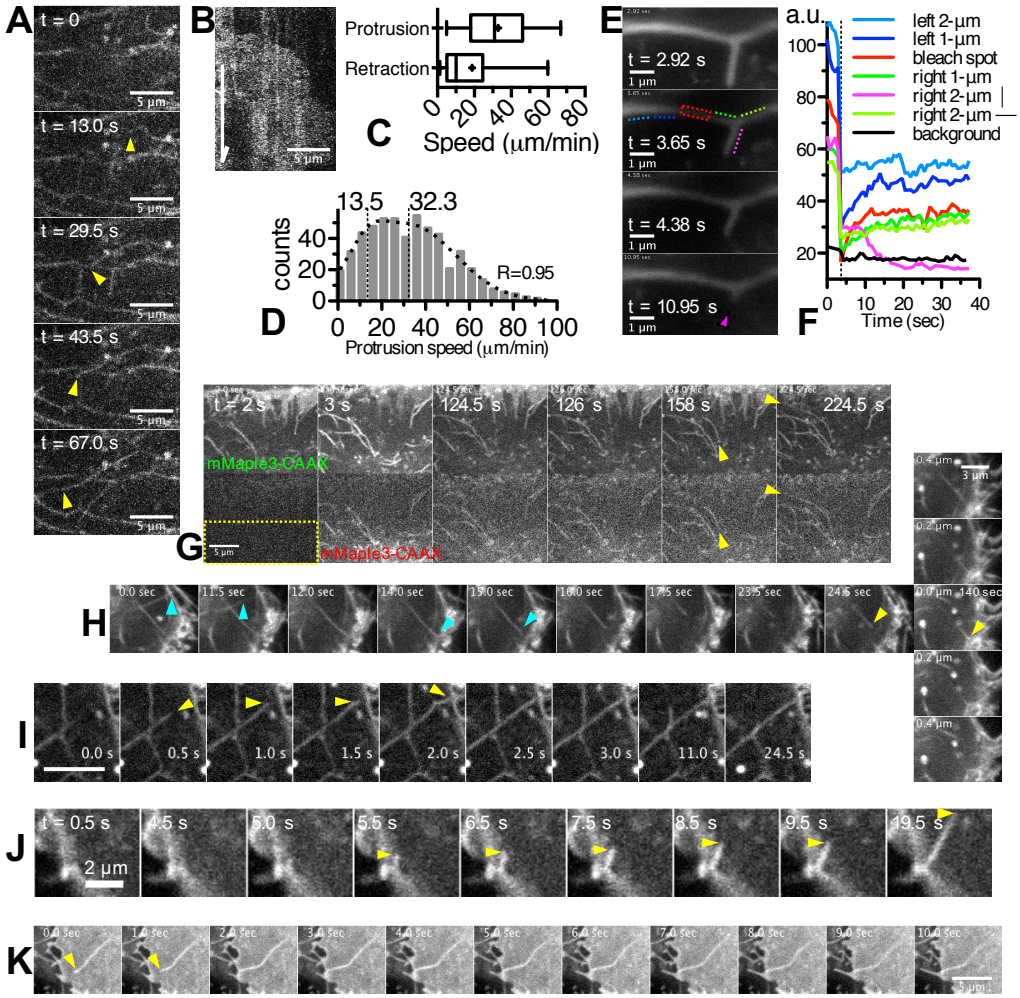
A
t = 0
t = 13.0 s
t = 29.5 s
t = 43.5 s
t = 67.0 s
5 μm
B
C
Protrusion
Retraction
0
20
40
60
80
Speed (μm/min)
D
13.5
32.3
counts
40
20
0
R=0.95
0
20
40
60
80
100
Protrusion speed (μm/min)
E
t = 2.92 s
t = 3.65 s
t = 4.38 s
t = 10.95 s
1 μm
F
a.u.
100
80
60
40
20
0
10
20
30
40
Time (sec)
left 2-μm
left 1-μm
bleach spot
right 1-μm
right 2-μm
right 2-μm
background
G
t = 2 s
3 s
124.5 s
126 s
158 s
224.5 s
mMaple3-CAAX
mMaple3-CAAX
5 μm
H
0.0 sec
11.5 sec
12.0 sec
14.0 sec
19.0 sec
18.0 sec
17.5 sec
23.5 sec
24.5 sec
I
0.0 s
0.5 s
1.0 s
1.5 s
2.0 s
2.5 s
3.0 s
11.0 s
24.5 s
J
t = 0.5 s
4.5 s
5.0 s
5.5 s
6.5 s
7.5 s
8.5 s
9.5 s
19.5 s
2 μm
K
5 μm

673 **Figure 4. The plasma membrane tubes are uncharacterized**
674 **membrane structures.**

675 A- HeLa cells expressing RFP-CAAX and GFP-CD9 were lively imaged by SDCM.
676 Scale bar = 5 μm.

677 B- HeLa cells expressing RFP-CAAX and GFP-Rab1a were lively imaged by SDCM.
678 Maximum intensity projection of a timelapse is displayed on the left, with expanded
679 view of yellow dash line boxed region on the right. Pink arrowhead indicates a
680 protruding GFP-Rab1 positive tube, and yellow arrowhead indicates a protruding
681 RFP-CAAX positive tube.

682 C- HeLa cells expressing markers for the plasma membrane and mitochondria (mito)
683 were lively imaged by SDCM.

684 D- HeLa cells expressing markers for the plasma membrane and endoplasmic
685 reticulum (ER) were lively imaged by SDCM. Five different markers for the
686 endoplasmic reticulum were used: calreticulin (CALR), ERD-2-like protein 1 (ELP),
687 GFP fusion with KDEL sequence (ER5), Sec61b and reticulon 4a (Rtn4a).

688 E- HeLa cells expressing GFP-CAAX and RFP-Sec61b were co-transfected with
689 either atlastin-1(K80A) or CLIMP-63, and lively imaged by SDCM.

690 F,F'- For cells as in (E), the length of the tube was divided by the long cell axis, the
691 area of ER sheets was divided by the area of the cell, or the number of tubes in the
692 cell was counted, and the percentage presented as box and whisker plots. One-way
693 ANOVA reports the difference is not significant (ns).

694 G- HeLa cells expressing markers for the plasma membrane and known organelles
695 were lively imaged by SDCM. Six different markers for five known organelles were
696 used: autophagosome (LC3), peroxisome (PXMP2), lysosome (LAMP1), early
697 endosome (Rab5a, Rab5b) and late endosome (Rab7a).

698 H- HeLa cells expressing GFP-CAAX were fixed, stained with antibody against a *cis*-
699 Golgi matrix protein (GM130), and imaged by SDCM. Slices of a Z stack from optical
700 sectioning are presented as montage.

701 I- SiT, a marker for the trans-Golgi network, was fused with 10xV4, co-expressed
702 with ^{SunTag}CAAX in HeLa cells, and lively imaged by SDCM. Slices of a Z stack from
703 optical sectioning are presented as montage. Yellow arrowheads indicate the double
704 positive tubes.

705

Figure 4

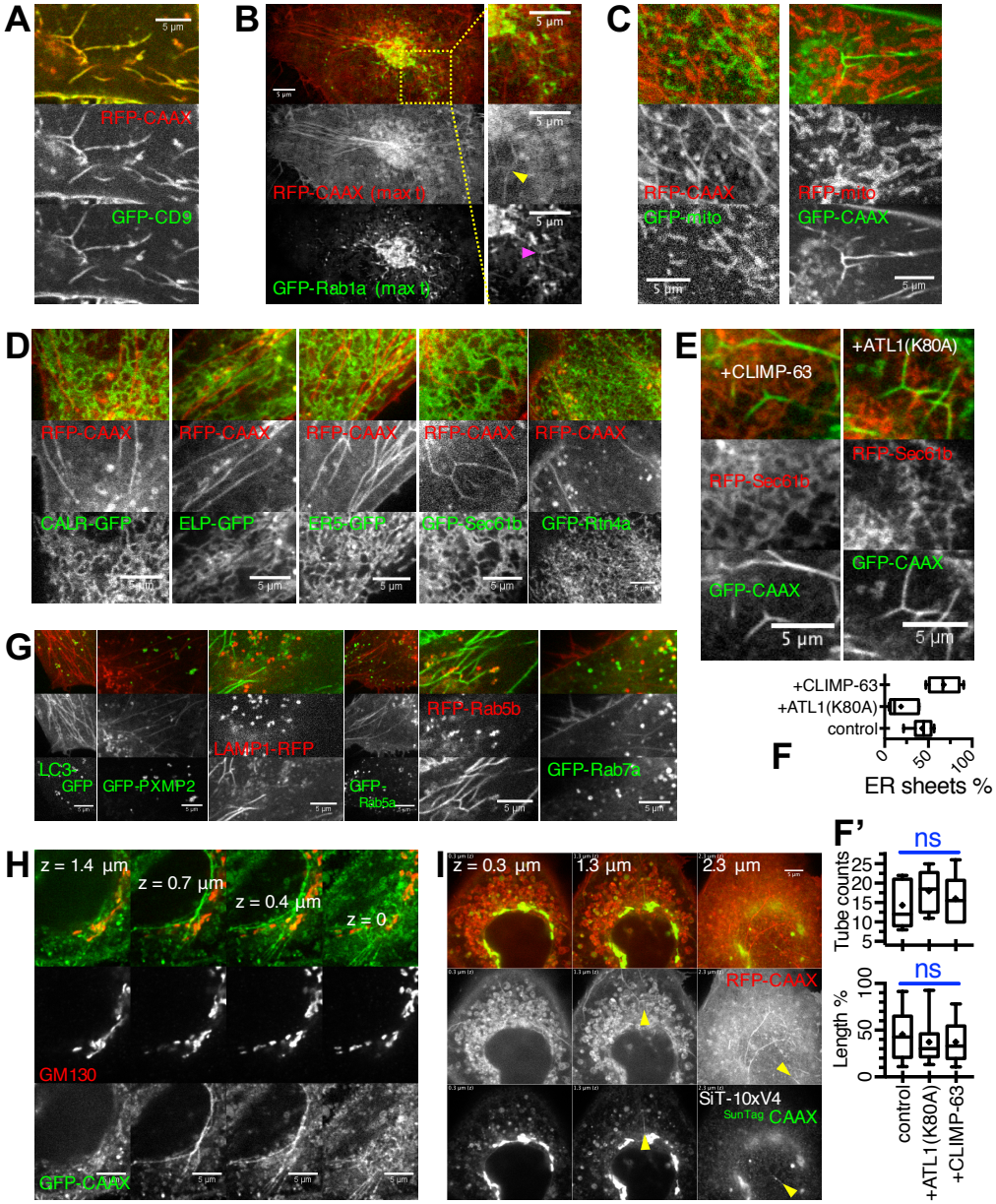
A
RFP-CAAX
GFP-CD9
B
RFP-CAAX (max I)
GFP-Rab1a (max I)
C
RFP-CAAX
GFP-mito
RFP-mito
GFP-CAAX
D
RFP-CAAX
CALR-GFP
ELP-GFP
ERS-GFP
GFP-Sec61b
GFP-Rtn4a
E
+CLIMP-63
+ATL1(K80A)
RFP-Sec61b
GFP-CAAX
5 µm
F
+CLIMP-63
+ATL1(K80A)
control
0
50
100
ER sheets %
G
LC3-GFP
GFP-PXMP2
LAMP1-RFP
GFP-Rab5a
RFP-Rab5b
GFP-Rab7a
H
z = 1.4 µm
z = 0.7 µm
z = 0.4 µm
z = 0
GM130
GFP-CAAX
I
z = 0.3 µm
1.3 µm
2.3 µm
RFP-CAAX
SiT-10xV4
SunTag
CAAX
F'
ns
Tube counts
25
20
15
10
5
ns
Length %
100
50
0
control
+ATL1(K80A)
+CLIMP-63

706 **Figure 5. Regulation of the dynamics of the plasma membrane**
707 **tubes.**

708 A- HeLa cells expressing GFP-CAAX and LifeAct-RFP were lively imaged by SDCM
709 and presented as timelapse montage. Yellow arrowheads indicate one end of a
710 protruding tube. Scale bar = 5 μm.

711 B- For cells as in (A), slices of a Z stack from optical sectioning are presented as
712 montage. Yellow arrowhead indicates a double positive tube, and open arrowhead
713 indicates a tube without LifeAct-RFP fluorescence.

714 C- For cells as in (A), timelapse images are presented as montage. Yellow
715 arrowheads indicate a tube retracts, turns, and protrudes. Open arrowhead indicates
716 a disassembling actin filament.

717 D- For the cell in (C), maximum intensity projection of its timelapse is displayed on
718 the up left corner, with kymographs from the pink lines displayed on the right and in
719 the lower panels. The cyan dash line indicates the time when the actin filament
720 disassembled but the tube had not retracted. Horizontal lines = 5 μm; vertical lines =
721 1 min.

722 E- HeLa cells as in (A) were treated with 20 μM latrunculin B for 30 min, imaged by
723 SDCM and presented as timelapse montage.

724 F- For cells as in (A), the length of the tube and the number of tubes in the cell,
725 before and after 20 μM latrunculin B (LatB) or 200 nM cytochalasin D (CytD) 30-min
726 treatment, was measured or counted, grouped by the experiments and presented as
727 mean ± 95% confidence intervals.

728 G- For cells expressing RFP-CAAX and GFP-αTubulin were lively imaged by SDCM
729 and regions from four different cells are displayed.

730 H- For cells as in (G), the number of protruding tubes and its percentage of the total
731 number of tubes, before and after 10 μM nocodazole or 2 μM paclitaxel 30-min
732 treatment, was counted or calculated, grouped by the experiments and presented as
733 mean ± 95% confidence intervals.

734 I- HeLa cells expressing RFP-CAAX and EB1-GFP were lively imaged by SDCM and
735 presented as timelapse montage. Yellow arrowhead indicates one end of a
736 protruding tube. Kymograph of the protruding tube is displayed on the right.
737 Horizontal line = 5 μm; vertical line = 30 sec.

738 J- HeLa cells expressing RFP-CAAX were fixed and stained with filipin. Regions from
739 four different cells are displayed. Yellow arrowheads indicate some double positive
740 tubes.

741 K- For cells as in (J), the length of RFP-CAAX positive tubes and their filipin stained
742 percentage were presented as scatter plot.

743 L- HeLa cells expressing RFP-CAAX were incubated with dehydroergosterol (DHE),
744 lively imaged by SDCM and presented as timelapse montage. Regions from two
745 different cells are displayed. Yellow arrowheads indicate double positive tubes, and
746 open arrowhead indicates a dynamic tube without DHE labeling.

747

Figure 5

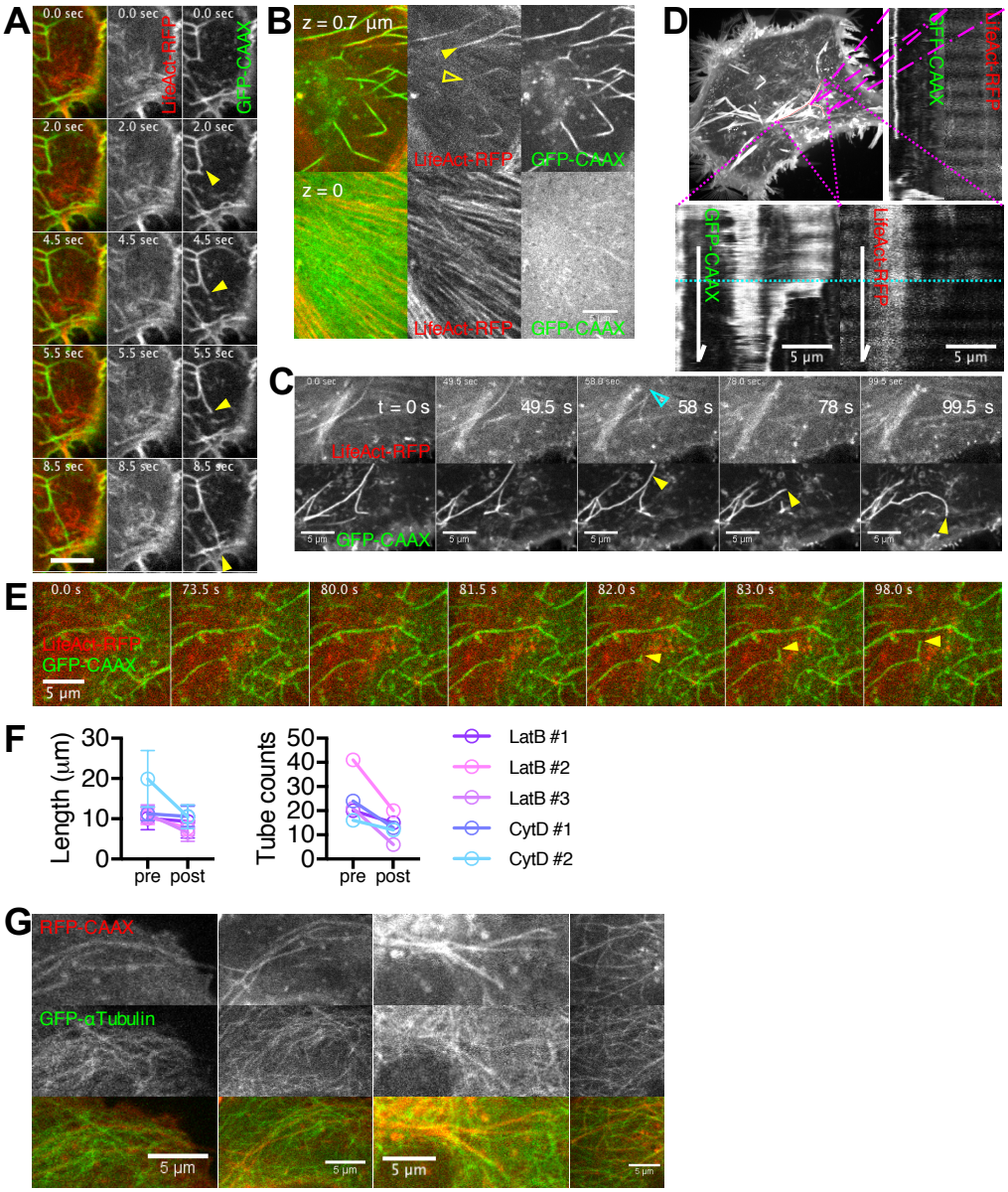
A
0.0 sec
2.0 sec
4.5 sec
5.5 sec
8.5 sec
LifeAct-RFP
GFP-CAAX
B
z = 0.7 μm
z = 0
LifeAct-RFP
GFP-CAAX
D
5 μm
C
t = 0 s
49.5 s
58 s
78 s
99.5 s
E
0.0 s
73.5 s
80.0 s
81.5 s
82.0 s
83.0 s
98.0 s
F
Length (μm)
Tube counts
pre
post
LatB #1
LatB #2
LatB #3
CytD #1
CytD #2
G
RFP-CAAX
GFP-αTubulin

Figure 5 (con't)

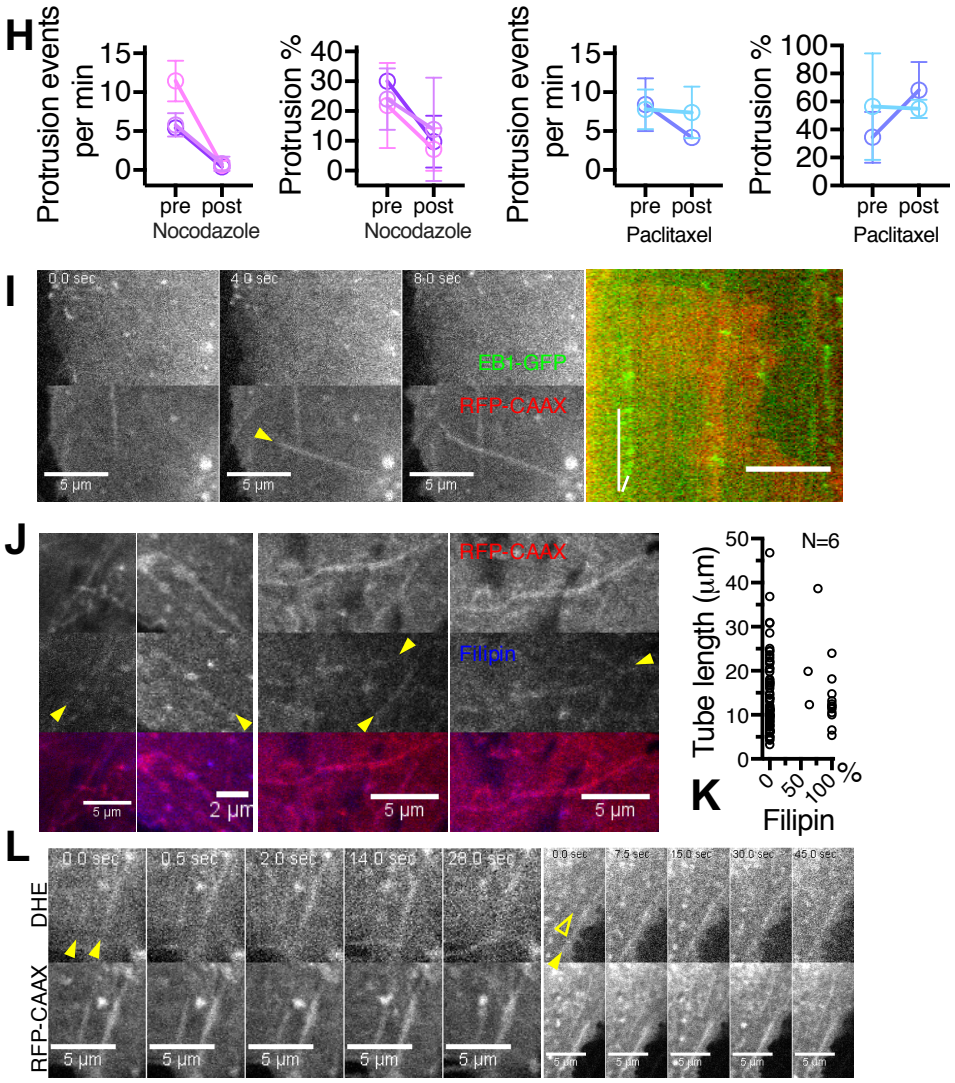

748 **Figure 6. The plasma membrane tubes are the preferred sites to**
749 **connect the endoplasmic reticulum to the plasma membrane.**

750 A- HeLa cells expressing RFP-CAAX and GFP–E-Syt1 were fixed and imaged by
751 SDCM. Regions from three different cells are displayed. Scale bar = 5 μm.

752 B- HeLa cells as in (A) were treated with 200 nM thapsigargin (TG) for 20 sec, fixed
753 and imaged by SDCM. Yellow arrowheads indicate GFP–E-Syt1 dots enriched on
754 tubes.

755 C- HeLa cells expressing RFP-CAAX, GFP–E-Syt1 and EBFP2-Sec61b were fixed
756 and imaged by SDCM. Regions from two different cells are displayed.

757 D- HeLa cells as in (C) were treated with 200 nM thapsigargin (TG) for 20 sec, fixed
758 and imaged by SDCM. Regions from three different cells are displayed.

759 E- HeLa cells expressing RFP-CAAX and GFP–E-Syt3 were fixed and imaged by
760 SDCM.

761 F- For cells as in (E), slices of a Z stack from optical sectioning are presented as
762 montage. Yellow arrowhead indicates a GFP–E-Syt3 dot colocalizes with a tube.

763 G- HeLa cells as in (E) were treated with 200 nM thapsigargin (TG) for 20 sec, fixed
764 and imaged by SDCM. Yellow arrowheads indicate spilled green fluorescence out of
765 the cells.

766 H- For cells in (A-G), the percentage of tubes enriched with ER-PM contact sites,
767 marked by either GFP–E-Syt1 or GFP–E-Syt3, were presented as mean ± standard
768 error of the mean.

769 I- For cells in (H), the density of total ER-PM contact sites in randomly selected
770 regions and the percentage of those ER-PM contact sites colocalizing with tubes
771 were presented as scatter plot.

772

Figure 6

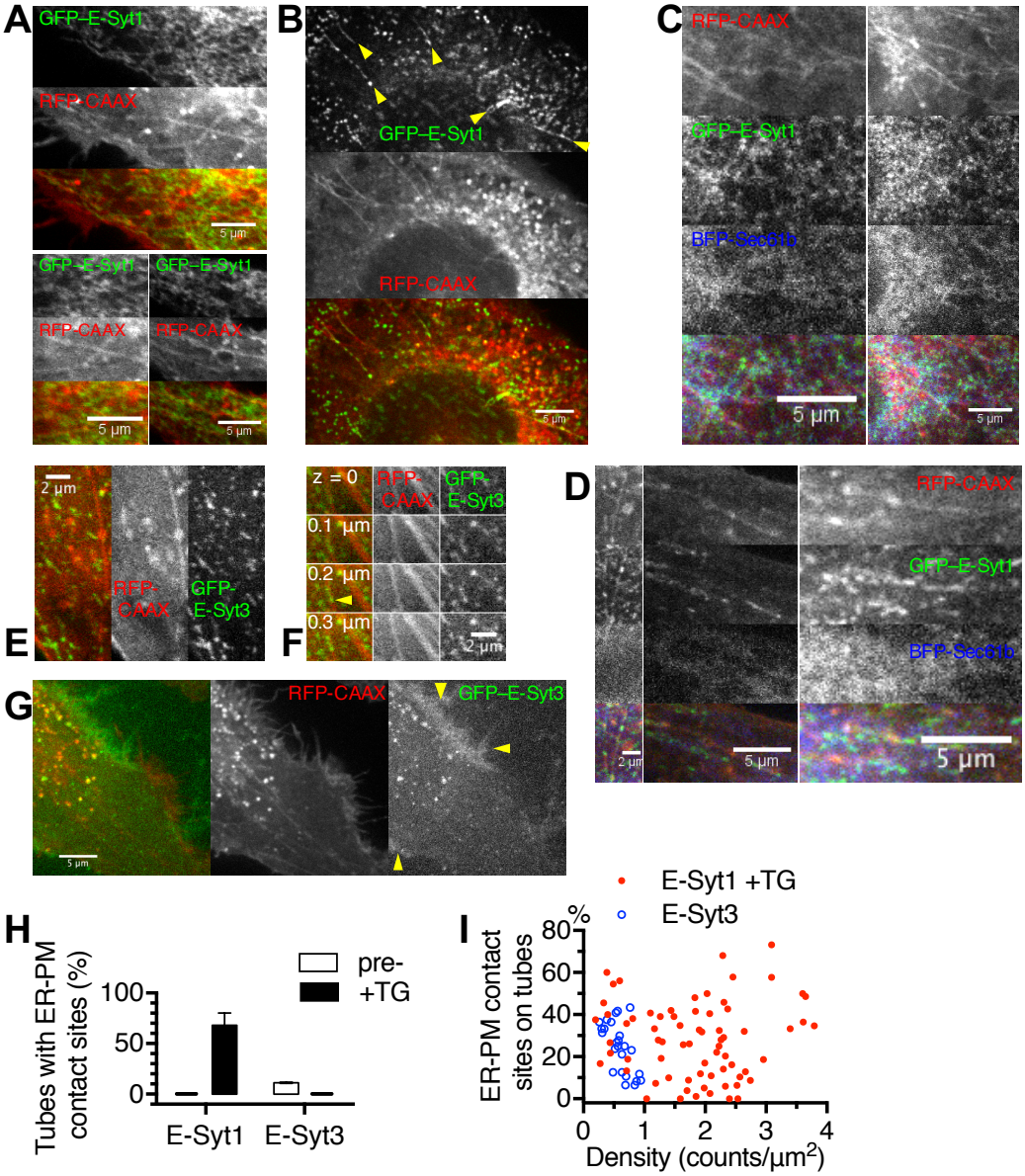
A
GFP-E-Syt1
RFP-CAAX
5 μm
B
GFP-E-Syt1
RFP-CAAX
C
RFP-CAAX
GFP-E-Syt1
BFP-Sec61b
5 μm
D
RFP-CAAX
GFP-E-Syt1
BFP-Sec61b
2 μm
5 μm
E
2 μm
RFP-CAAX
GFP-E-Syt3
F
z = 0
0.1 μm
0.2 μm
0.3 μm
2 μm
G
RFP-CAAX
GFP-E-Syt3
5 μm
H
Tubes with ER-PM contact sites (%)
100
50
0
pre-
+TG
E-Syt1
E-Syt3
I
E-Syt1 +TG
E-Syt3
%
ER-PM contact sites on tubes
80
60
40
20
0
0
1
2
3
4
Density (counts/μm2)

773 **Figure 7. The plasma membrane tubes facilitate receptor**
774 **presentation to the surface of cells.**

775 A- HeLa cells expressing GFP-CAAX were immunolabeled by antibody against
776 GLUT1 and imaged by SDCM. Z stacks from optical sectioning were combined by
777 wavelet-based extended depth of focus projection and presented with pseudo colors,
778 GLUT1 in red and GFP-CAAX in green. Expanded views of yellow dash lines boxed
779 region are displayed in the lower panels. Scale bar = 5 μm.

780 B,B'- HeLa cells as in (A) were glucose-deprived for 12 hr, processed and presented
781 as in (A). Four different regions are displayed in B' in expanded view.

782 C,G- HeLa cells expressing GFP-CAAX were treated under different conditions,
783 fixed, immunolabeled by antibody against either GLUT1 or EGFR, and imaged by
784 SDCM. The percentage of tubes positive for GLUT1/EGFR are presented as scatter
785 dot plots, with mean ± 95% confidence intervals. Turkey multiple comparison test
786 was used after one-way ANOVA to generate the p values (****, P<0.0001; ***,
787 P<0.001; **, P<0.01; *, P<0.05; ns, not significant). Glc is the abbreviation for
788 glucose.

789 D,H- For cells in (C,G), the average pixel intensity of GLUT1/EGFR on the plasma
790 membrane divided by the background are presented as scatter dot plots, and
791 statistically analyzed as in (C,G).

792 E,F- For cells in (C), the number of tubes in the cell or the length of tubes was
793 counted or measured, and presented as scatter dot plots. One-way ANOVA reports
794 the difference is not significant (ns).

795

Figure 7

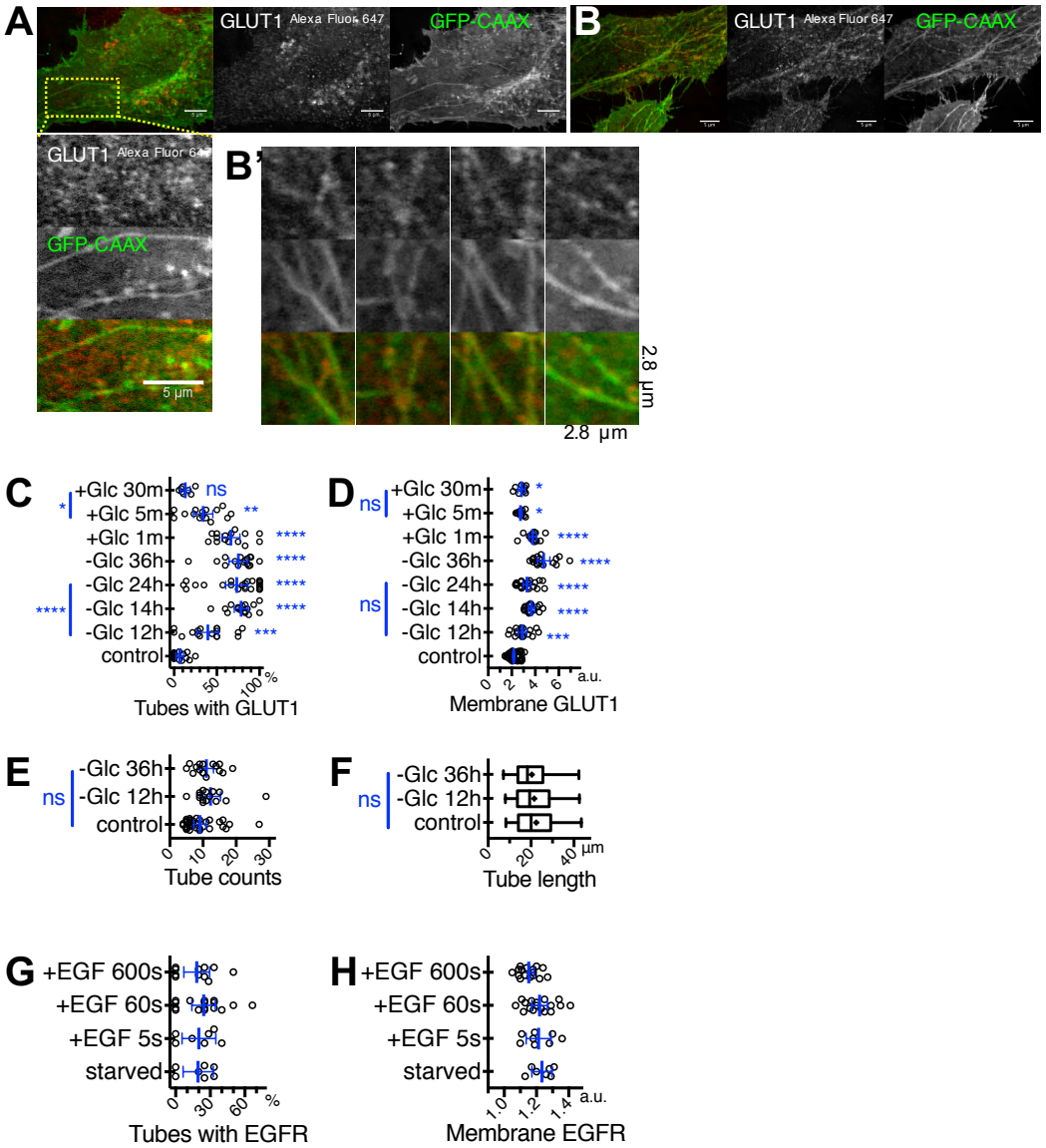
A
GLUT1 Alexa Fluor 647
GFP-CAAX
B
GLUT1 Alexa Fluor 647
GFP-CAAX
GLUT1 Alexa Fluor 647
GFP-CAAX
5 µm
B'
2.8 µm
2.8 µm
C
+Glc 30m
+Glc 5m
+Glc 1m
-Glc 36h
-Glc 24h
-Glc 14h
-Glc 12h
control
ns
*
**
****
***
0
50
100
%
Tubes with GLUT1
D
+Glc 30m
+Glc 5m
+Glc 1m
-Glc 36h
-Glc 24h
-Glc 14h
-Glc 12h
control
ns
*
****
***
0
2
4
6
a.u.
Membrane GLUT1
E
-Glc 36h
-Glc 12h
control
ns
0
10
20
30
Tube counts
F
-Glc 36h
-Glc 12h
control
ns
0
20
40
µm
Tube length
G
+EGF 600s
+EGF 60s
+EGF 5s
starved
0
30
60
%
Tubes with EGFR
H
+EGF 600s
+EGF 60s
+EGF 5s
starved
1.0
1.2
1.4
a.u.
Membrane EGFR

References

Allan, V., and Vale, R. (1994). Movement of membrane tubules along microtubules in vitro: evidence for specialised sites of motor attachment. J Cell Sci *107 (Pt 7)*, 1885-1897.

Allan, V.J., and Vale, R.D. (1991). Cell cycle control of microtubule-based membrane transport and tubule formation in vitro. J Cell Biol *113*, 347-359.

Almeida, C.G., Yamada, A., Tenza, D., Louvard, D., Raposo, G., and Coudrier, E. (2011). Myosin 1b promotes the formation of post-Golgi carriers by regulating actin assembly and membrane remodelling at the trans-Golgi network. Nat Cell Biol *13*, 779-789.

Anitei, M., Stange, C., Parshina, I., Baust, T., Schenck, A., Raposo, G., Kirchhausen, T., and Hoflack, B. (2010). Protein complexes containing CYFIP/Sra/PIR121 coordinate Arf1 and Rac1 signalling during clathrin-AP-1-coated carrier biogenesis at the TGN. Nat Cell Biol *12*, 330-340.

Antonescu, C.N., Danuser, G., and Schmid, S.L. (2010). Phosphatidic acid plays a regulatory role in clathrin-mediated endocytosis. Mol Biol Cell *21*, 2944-2952.

Apolloni, A., Prior, I.A., Lindsay, M., Parton, R.G., and Hancock, J.F. (2000). H-ras but not K-ras traffics to the plasma membrane through the exocytic pathway. Mol Cell Biol *20*, 2475-2487.

Blobel, G. (2000). Protein targeting (Nobel lecture). Chembiochem *1*, 86-102.

Bonifacino, J.S., and Glick, B.S. (2004). The mechanisms of vesicle budding and fusion. Cell *116*, 153-166.

Cai, L., Makhov, A.M., Schafer, D.A., and Bear, J.E. (2008). Coronin 1B antagonizes cortactin and remodels Arp2/3-containing actin branches in lamellipodia. Cell *134*, 828-842.

Cai, L., Marshall, T.W., Uetrecht, A.C., Schafer, D.A., and Bear, J.E. (2007). Coronin 1B coordinates Arp2/3 complex and cofilin activities at the leading edge. Cell *128*, 915-929.

Chen, B.C., Legant, W.R., Wang, K., Shao, L., Milkie, D.E., Davidson, M.W., Janetopoulos, C., Wu, X.S., Hammer, J.A., 3rd, Liu, Z.*, et al.* (2014). Lattice light-sheet microscopy: imaging molecules to embryos at high spatiotemporal resolution. Science *346*, 1257998.

Chinnapen, D.J., Hsieh, W.T., te Welscher, Y.M., Saslowsky, D.E., Kaoutzani, L., Brandsma, E., D'Auria, L., Park, H., Wagner, J.S., Drake, K.R.*, et al.* (2012). Lipid sorting by ceramide structure from plasma membrane to ER for the cholera toxin receptor ganglioside GM1. Dev Cell *23*, 573-586.

832 Choy, E., Chiu, V.K., Silletti, J., Feoktistov, M., Morimoto, T., Michaelson, D., Ivanov,
833 I.E., and Philips, M.R. (1999). Endomembrane trafficking of ras: the CAAX motif
834 targets proteins to the ER and Golgi. Cell *98*, 69-80.

835 Cooper, M.S., Cornell-Bell, A.H., Chernjavsky, A., Dani, J.W., and Smith, S.J. (1990).
836 Tubulovesicular processes emerge from trans-Golgi cisternae, extend along
837 microtubules, and interlink adjacent trans-golgi elements into a reticulum. Cell *61*,
838 135-145.

839 Dale, R.M., and Topczewski, J. (2011). Identification of an evolutionarily conserved
840 regulatory element of the zebrafish col2a1a gene. Dev Biol *357*, 518-531.

841 Du, W., Su, Q.P., Chen, Y., Zhu, Y., Jiang, D., Rong, Y., Zhang, S., Zhang, Y., Ren,
842 H., Zhang, C*., et al.* (2016). Kinesin 1 Drives Autolysosome Tubulation. Dev Cell *37*,
843 326-336.

844 Dubey, G.P., and Ben-Yehuda, S. (2011). Intercellular nanotubes mediate bacterial
845 communication. Cell *144*, 590-600.

846 Feng, Y., Jadhav, A.P., Rodighiero, C., Fujinaga, Y., Kirchhausen, T., and Lencer,
847 W.I. (2004). Retrograde transport of cholera toxin from the plasma membrane to the
848 endoplasmic reticulum requires the trans-Golgi network but not the Golgi apparatus
849 in Exo2-treated cells. EMBO Rep *5*, 596-601.

850 Fernandez-Busnadiego, R., Saheki, Y., and De Camilli, P. (2015). Three-dimensional
851 architecture of extended synaptotagmin-mediated endoplasmic reticulum-plasma
852 membrane contact sites. Proc Natl Acad Sci U S A *112*, E2004-2013.

853 Fletcher, D.A., and Mullins, R.D. (2010). Cell mechanics and the cytoskeleton.
854 Nature *463*, 485-492.

855 Friedman, J.R., Lackner, L.L., West, M., DiBenedetto, J.R., Nunnari, J., and Voeltz,
856 G.K. (2011). ER tubules mark sites of mitochondrial division. Science *334*, 358-362.

857 Gallione, C.J., and Rose, J.K. (1985). A single amino acid substitution in a
858 hydrophobic domain causes temperature-sensitive cell-surface transport of a mutant
859 viral glycoprotein. J Virol *54*, 374-382.

860 Ganley, I.G., Espinosa, E., and Pfeffer, S.R. (2008). A syntaxin 10-SNARE complex
861 distinguishes two distinct transport routes from endosomes to the trans-Golgi in
862 human cells. J Cell Biol *180*, 159-172.

863 Giordano, F., Saheki, Y., Idevall-Hagren, O., Colombo, S.F., Pirruccello, M.,
864 Milosevic, I., Gracheva, E.O., Bagriantsev, S.N., Borgese, N., and De Camilli, P.
865 (2013). PI(4,5)P(2)-dependent and Ca(2+)-regulated ER-PM interactions mediated
866 by the extended synaptotagmins. Cell *153*, 1494-1509.

867 Hao, M., Lin, S.X., Karylowski, O.J., Wustner, D., McGraw, T.E., and Maxfield, F.R.
868 (2002). Vesicular and non-vesicular sterol transport in living cells. J Biol Chem *277*,
869 609-617.

870 Hattula, K., Furuhjelm, J., Tikkanen, J., Tanhuanpaa, K., Laakkonen, P., and
871 Peranen, J. (2006). Characterization of the Rab8-specific membrane traffic route
872 linked to protrusion formation. J Cell Sci *119*, 4866-4877.

873 Hopkins, C.R., Gibson, A., Shipman, M., and Miller, K. (1990). Movement of
874 internalized ligand-receptor complexes along a continuous endosomal reticulum.
875 Nature *346*, 335-339.

876 Howes, M.T., Kirkham, M., Riches, J., Cortese, K., Walser, P.J., Simpson, F., Hill,
877 M.M., Jones, A., Lundmark, R., Lindsay, M.R.*, et al.* (2010). Clathrin-independent
878 carriers form a high capacity endocytic sorting system at the leading edge of
879 migrating cells. J Cell Biol *190*, 675-691.

880 Hu, J., Shibata, Y., Zhu, P.P., Voss, C., Rismanchi, N., Prinz, W.A., Rapoport, T.A.,
881 and Blackstone, C. (2009). A class of dynamin-like GTPases involved in the
882 generation of the tubular ER network. Cell *138*, 549-561.

883 Huang, X., Sun, L., Ji, S., Zhao, T., Zhang, W., Xu, J., Zhang, J., Wang, Y., Wang,
884 X., Franzini-Armstrong, C.*, et al.* (2013). Kissing and nanotunneling mediate
885 intermitochondrial communication in the heart. Proc Natl Acad Sci U S A *110*, 2846-
886 2851.

887 Hutagalung, A.H., and Novick, P.J. (2011). Role of Rab GTPases in membrane traffic
888 and cell physiology. Physiol Rev *91*, 119-149.

889 Ishikawa, H., and Marshall, W.F. (2011). Ciliogenesis: building the cell's antenna. Nat
890 Rev Mol Cell Biol *12*, 222-234.

891 Klopfenstein, D.R., Klumperman, J., Lustig, A., Kammerer, R.A., Oorschot, V., and
892 Hauri, H.P. (2001). Subdomain-specific localization of CLIMP-63 (p63) in the
893 endoplasmic reticulum is mediated by its luminal alpha-helical segment. J Cell Biol
894 *153*, 1287-1300.

895 Kreitzer, G., Schmoranzer, J., Low, S.H., Li, X., Gan, Y., Weimbs, T., Simon, S.M.,
896 and Rodriguez-Boulan, E. (2003). Three-dimensional analysis of post-Golgi carrier
897 exocytosis in epithelial cells. Nat Cell Biol *5*, 126-136.

898 Kwok, E.Y., and Hanson, M.R. (2004). Stromules and the dynamic nature of plastid
899 morphology. J Microsc *214*, 124-137.

900 Lippincott-Schwartz, J. (2011). An evolving paradigm for the secretory pathway? Mol
901 Biol Cell *22*, 3929-3932.

902 Lippincott-Schwartz, J., Donaldson, J.G., Schweizer, A., Berger, E.G., Hauri, H.P.,
903 Yuan, L.C., and Klausner, R.D. (1990). Microtubule-dependent retrograde transport
904 of proteins into the ER in the presence of brefeldin A suggests an ER recycling
905 pathway. Cell *60*, 821-836.

906 Lippincott-Schwartz, J., Roberts, T.H., and Hirschberg, K. (2000). Secretory protein
907 trafficking and organelle dynamics in living cells. Annu Rev Cell Dev Biol *16*, 557-
908 589.

909 Luini, A., Mironov, A.A., Polishchuk, E.V., and Polishchuk, R.S. (2008).
910 Morphogenesis of post-Golgi transport carriers. Histochem Cell Biol *129*, 153-161.

911 Manford, A.G., Stefan, C.J., Yuan, H.L., Macgurn, J.A., and Emr, S.D. (2012). ER-to-
912 plasma membrane tethering proteins regulate cell signaling and ER morphology. Dev
913 Cell *23*, 1129-1140.

914 Mesmin, B., Pipalia, N.H., Lund, F.W., Ramlall, T.F., Sokolov, A., Eliezer, D., and
915 Maxfield, F.R. (2011). STARD4 abundance regulates sterol transport and sensing.
916 Mol Biol Cell *22*, 4004-4015.

917 Moreira, K.E., Walther, T.C., Aguilar, P.S., and Walter, P. (2009). Pil1 controls
918 eisosome biogenesis. Mol Biol Cell *20*, 809-818.

919 Mueckler, M., Caruso, C., Baldwin, S.A., Panico, M., Blench, I., Morris, H.R., Allard,
920 W.J., Lienhard, G.E., and Lodish, H.F. (1985). Sequence and structure of a human
921 glucose transporter. Science *229*, 941-945.

922 Natesan, S.K., Sullivan, J.A., and Gray, J.C. (2005). Stromules: a characteristic cell-
923 specific feature of plastid morphology. J Exp Bot *56*, 787-797.

924 Nishiyama, M., Higuchi, H., and Yanagida, T. (2002). Chemomechanical coupling of
925 the forward and backward steps of single kinesin molecules. Nat Cell Biol *4*, 790-797.

926 Parsons, S.F., and Salmon, E.D. (1997). Microtubule assembly in clarified Xenopus
927 egg extracts. Cell Motil Cytoskeleton *36*, 1-11.

928 Peters, R. (1984). Nucleo-cytoplasmic flux and intracellular mobility in single
929 hepatocytes measured by fluorescence microphotolysis. EMBO J *3*, 1831-1836.

930 Peterson, S.J., and Krasnow, M.A. (2015). Subcellular trafficking of FGF controls
931 tracheal invasion of Drosophila flight muscle. Cell *160*, 313-323.

932 Polishchuk, E.V., Di Pentima, A., Luini, A., and Polishchuk, R.S. (2003). Mechanism
933 of constitutive export from the golgi: bulk flow via the formation, protrusion, and en
934 bloc cleavage of large trans-golgi network tubular domains. Mol Biol Cell *14*, 4470-
935 4485.

936 Presley, J.F., Cole, N.B., Schroer, T.A., Hirschberg, K., Zaal, K.J., and Lippincott-
937 Schwartz, J. (1997). ER-to-Golgi transport visualized in living cells. Nature *389*, 81-
938 85.

939 Raa, H., Grimmer, S., Schwudke, D., Bergan, J., Walchli, S., Skotland, T.,
940 Shevchenko, A., and Sandvig, K. (2009). Glycosphingolipid requirements for
941 endosome-to-Golgi transport of Shiga toxin. Traffic *10*, 868-882.

942 Reyes, A., He, J., Mao, C.C., Bailey, L.J., Di Re, M., Sembongi, H., Kazak, L.,
943 Dzionek, K., Holmes, J.B., Cluett, T.J.*, et al.* (2011). Actin and myosin contribute to
944 mammalian mitochondrial DNA maintenance. Nucleic Acids Res *39*, 5098-5108.

945 Roland, J.T., Kenworthy, A.K., Peranen, J., Caplan, S., and Goldenring, J.R. (2007).
946 Myosin Vb interacts with Rab8a on a tubular network containing EHD1 and EHD3.
947 Mol Biol Cell *18*, 2828-2837.

948 Rowland, A.A., Chitwood, P.J., Phillips, M.J., and Voeltz, G.K. (2014). ER contact
949 sites define the position and timing of endosome fission. Cell *159*, 1027-1041.

950 Rowland, A.A., and Voeltz, G.K. (2012). Endoplasmic reticulum-mitochondria
951 contacts: function of the junction. Nat Rev Mol Cell Biol *13*, 607-625.

952 Russo, A.J., Mathiowetz, A.J., Hong, S., Welch, M.D., and Campellone, K.G. (2016).
953 Rab1 recruits WHAMM during membrane remodeling but limits actin nucleation. Mol
954 Biol Cell *27*, 967-978.

955 Rustom, A., Saffrich, R., Markovic, I., Walther, P., and Gerdes, H.H. (2004).
956 Nanotubular highways for intercellular organelle transport. Science *303*, 1007-1010.

957 Sabharanjak, S., Sharma, P., Parton, R.G., and Mayor, S. (2002). GPI-anchored
958 proteins are delivered to recycling endosomes via a distinct cdc42-regulated, clathrin-
959 independent pinocytic pathway. Dev Cell *2*, 411-423.

960 Schauder, C.M., Wu, X., Saheki, Y., Narayanaswamy, P., Torta, F., Wenk, M.R., De
961 Camilli, P., and Reinisch, K.M. (2014). Structure of a lipid-bound extended
962 synaptotagmin indicates a role in lipid transfer. Nature *510*, 552-555.

963 Schnitzer, M.J., Visscher, K., and Block, S.M. (2000). Force production by single
964 kinesin motors. Nat Cell Biol *2*, 718-723.

965 Sciaky, N., Presley, J., Smith, C., Zaal, K.J., Cole, N., Moreira, J.E., Terasaki, M.,
966 Siggia, E., and Lippincott-Schwartz, J. (1997). Golgi tubule traffic and the effects of
967 brefeldin A visualized in living cells. J Cell Biol *139*, 1137-1155.

968 Sherer, N.M., Lehmann, M.J., Jimenez-Soto, L.F., Ingmundson, A., Horner, S.M.,
969 Cicchetti, G., Allen, P.G., Pypaert, M., Cunningham, J.M., and Mothes, W. (2003).
970 Visualization of retroviral replication in living cells reveals budding into multivesicular
971 bodies. Traffic *4*, 785-801.

972 Simons, K., and Toomre, D. (2000). Lipid rafts and signal transduction. Nat Rev Mol
973 Cell Biol *1*, 31-39.

974 Stefan, C.J., Manford, A.G., Baird, D., Yamada-Hanff, J., Mao, Y., and Emr, S.D.
975 (2011). Osh proteins regulate phosphoinositide metabolism at ER-plasma membrane
976 contact sites. Cell *144*, 389-401.

977 Steinman, R.M., Mellman, I.S., Muller, W.A., and Cohn, Z.A. (1983). Endocytosis and
978 the recycling of plasma membrane. J Cell Biol *96*, 1-27.

979 Swanson, J., Bushnell, A., and Silverstein, S.C. (1987). Tubular lysosome
980 morphology and distribution within macrophages depend on the integrity of
981 cytoplasmic microtubules. Proc Natl Acad Sci U S A *84*, 1921-1925.

982 Tanenbaum, M.E., Gilbert, L.A., Qi, L.S., Weissman, J.S., and Vale, R.D. (2014). A
983 protein-tagging system for signal amplification in gene expression and fluorescence
984 imaging. Cell *159*, 635-646.

985 Tavassoli, S., Chao, J.T., Young, B.P., Cox, R.C., Prinz, W.A., de Kroon, A.I., and
986 Loewen, C.J. (2013). Plasma membrane--endoplasmic reticulum contact sites
987 regulate phosphatidylcholine synthesis. EMBO Rep *14*, 434-440.

988 Tooze, J., and Hollinshead, M. (1991). Tubular early endosomal networks in AtT20
989 and other cells. J Cell Biol *115*, 635-653.

990 Tooze, J., and Hollinshead, M. (1992). In AtT20 and HeLa cells brefeldin A induces
991 the fusion of tubular endosomes and changes their distribution and some of their
992 endocytic properties. J Cell Biol *118*, 813-830.

993 Voeltz, G.K., and Prinz, W.A. (2007). Sheets, ribbons and tubules - how organelles
994 get their shape. Nat Rev Mol Cell Biol *8*, 258-264.

995 Voeltz, G.K., Prinz, W.A., Shibata, Y., Rist, J.M., and Rapoport, T.A. (2006). A class
996 of membrane proteins shaping the tubular endoplasmic reticulum. Cell *124*, 573-586.

997 Wagner, M., Rajasekaran, A.K., Hanzel, D.K., Mayor, S., and Rodriguez-Boulan, E.
998 (1994). Brefeldin A causes structural and functional alterations of the trans-Golgi
999 network of MDCK cells. J Cell Sci *107 (Pt 4)*, 933-943.

1000 Waguri, S., Dewitte, F., Le Borgne, R., Rouille, Y., Uchiyama, Y., Dubremetz, J.F.,
1001 and Hoflack, B. (2003). Visualization of TGN to endosome trafficking through
1002 fluorescently labeled MPR and AP-1 in living cells. Mol Biol Cell *14*, 142-155.

1003 Walther, T.C., Brickner, J.H., Aguilar, P.S., Bernales, S., Pantoja, C., and Walter, P.
1004 (2006). Eisosomes mark static sites of endocytosis. Nature *439*, 998-1003.

1005 Wang, C., Du, W., Su, Q.P., Zhu, M., Feng, P., Li, Y., Zhou, Y., Mi, N., Zhu, Y., Jiang,
1006 D.*, et al.* (2015). Dynamic tubulation of mitochondria drives mitochondrial network
1007 formation. Cell Res *25*, 1108-1120.

1008 Wang, S., Moffitt, J.R., Dempsey, G.T., Xie, X.S., and Zhuang, X. (2014).
1009 Characterization and development of photoactivatable fluorescent proteins for single-
1010 molecule-based superresolution imaging. Proc Natl Acad Sci U S A *111*, 8452-8457.

1011 Waterman-Storer, C.M., Gregory, J., Parsons, S.F., and Salmon, E.D. (1995).
1012 Membrane/microtubule tip attachment complexes (TACs) allow the assembly
1013 dynamics of plus ends to push and pull membranes into tubulovesicular networks in
1014 interphase Xenopus egg extracts. J Cell Biol *130*, 1161-1169.

1015 Yao, L., Zhou, L., Wang, J., Cai, L. (2017). Visualize cytoplasmic abundant protein
1016 localization via SunTag strategy. Journal of Fudan University (Natural Science) *56(5)*,
1017 588-595.

1018 Zambryski, P. (1995). Plasmodesmata: plant channels for molecules on the move.
1019 Science *270*, 1943-1944.